SGG SGS sc | nat
Swiss Journal of Geosciences

ORIGINAL PAPER Open Access

Deep hydrochemical section through the Central Alps: evolution of deep water in the continental upper crust and solute acquisition during water–rock-interaction along the Sedrun section of the Gotthard Base Tunnel

Ingrid Stober[1*], Federico Giovanoli[2], Victoria Wiebe[1] and Kurt Bucher[1]

Abstract

Drilling of the Gotthard Rail Base Tunnel through the Central Alps from 2005 to 2010 opened up fractured basement units and frequent water inflows provided access to the major fluid-rock interactions processes in orogenic crystalline upper crust. Construction of the 57 km long tunnel was divided into five different sections. Here we report data and observations from the 10 km long central Sedrun section 211 water samples were collected at inflow points 900 to 2350 m below the surface. The exceptional samples and data provide a comprehension of the hydrochemical evolution and solute acquisition of deep groundwater in basement units. The investigated tunnel section drilled through steeply dipping rock units and vertical fracture systems at high angle. It cuts across granite, gneiss and schist of the pre-Alpine basement and across two narrow zones of meta-sediments. Rock temperature along the Sedrun section varies from 30 to 45 °C depending on the thickness of the overburden. The fracture water is of meteoric origin and acquires its composition exclusively by chemical interaction with the surrounding rocks along the flow path. Water from inflow points in the basement of the Gotthard Massif has typically a high pH of about 10 and total dissolved solids in the range of 100 to 300 mg L^{-1}. Sodium is the prime cation of most waters. Although plentiful in the rocks, calcium, potassium and magnesium are low to very low in water. The anions associated with Na are carbonate/bicarbonate, sulfate, fluoride and chloride in widely varying proportions. High fluoride concentrations of up to 15.4 mg L^{-1} are characteristic for most waters. As a result of the high pH dissolved silica (SiO_2) reached concentrations of up to 58 mg L^{-1} and represents 25—30 wt% of the solutes. The meteoric recharge provides dissolved O_2 and CO_2 to the fluid-rock interaction processes. The solutes derive from the dissolution of feldspar (Na^+, SiO_{2aq}), oxidation of sulfides to sulfate (SO_4^{2-}), alteration of biotite (F^-), and fluid inclusions opened by brittle deformation (Cl^-). The solids formed during fluid-rock interaction, mainly zeolites, chlorite (and other clay minerals) and secondary Fe-minerals, remove Mg, Fe, and K almost quantitatively from the water. The high pH results from hydrolysis of silicates. The data distinctly

Editorial handling: Paola Manzotti.

*Correspondence: ingrid.stober@minpet.uni-freiburg.de
[1] Institut für Geo- und Umweltnaturwissenschaften, Albert-Ludwigs-Universität Freiburg, Albertstr. 23B, 79104 Freiburg, Germany
Full list of author information is available at the end of the article

show that within the depth interval of 1.0–2.5 km below surface deep water in continental basement evolves to a low TDS, high pH, sodium carbonate and silica solution by interaction of gneiss and granite with infiltrating pristine meteoric water, snow and rain.

Keywords: Crustal fluids, Water–rock interaction, Dissolution–precipitation, Gotthard base tunnel, Crystalline basement

1 Introduction

The fracture pore space of continental basement is usually filled with an aqueous fluid. The fractures form an interconnected framework of open permeable space and fluid movement follows the Darcy-flow law (Manning & Ingebritsen, 1999). The hydraulic conductivity of the fracture network is on the order of 10^{-9}–10^{-7} m s^{-1} (Stober, 1996). Significant advective fluid flow is possible if the necessary hydraulic gradients are present (Ingebritsen & Manning, 1999; Manning & Ingebritsen, 1999; Stober & Bucher, 2005, 2007).

The aqueous fluid present in the fracture porosity of the upper continental crust has a wide range of chemical composition and also a surprisingly diverse origin of solutes (Bucher & Stober, 2010; Edmunds et al., 1985; Frape et al., 2004; Gascoyne, 2004; Stotler et al., 2012). Basement water acquires its dissolved components mainly by reaction with minerals of the host rocks exposed along the fractures. The basement host rock is typically fractured granite and gneiss. These fluid-rock interaction processes (WRI) proceed until the water reaches chemical equilibrium with the host rock. However, migrating fluids may introduce water to the local environment with solutes that have been acquired from rocks or by chemical processes at some distance of the area of interest. The imported water then re-adjusts its composition again by reaction with its basement host rock. This common situation in continental basement complicates the evaluation of the origin and chemical development of observed water compositions enormously.

Rugged mountain topography is the key driver for meteoric water migration in non-magmatic orogenic belts (e.g. Forster & Smith, 1988; Ge et al., 2008; Goderniaux et al., 2013; Hubbert, 1940; Toth, 1963). Surface water from precipitation in high-mountains with exposed basement rocks infiltrates the fracture porosity of gneiss and granite and migrates through the rocks driven by topographic gradients. Along the downward flow-path the surface water reacts with the mineral assemblage exposed on the fracture surfaces in granite and gneiss thereby gradually reducing overall reaction affinity during reaction progress (Helgeson, 1979; Helgeson et al., 1969). Along the reaction path, minerals dissolve and precipitate and the water accumulates solutes. At low temperature, reaction progress is mainly controlled by the kinetics of dissolution and precipitation reactions. Most water–rock-interaction processes involve transport steps that link the site where unstable minerals dissolve with sites where more stable minerals precipitate (Bucher et al., 2012; Weisenberger & Bucher, 2011; Zhu, 2009). Water–rock interaction along flow paths in fractured mountainous basement proceeds with an initial water of known composition, namely the average composition of the annual local precipitation.

Upward migration of originally meteoric water in crystalline basement rocks may occur along deep-reaching faults or in areas with enhanced permeability as verified by the occurrence of thermal springs and their chemical and isotopic composition (Belgrano et al., 2016; Bucher et al., 2009; Craw et al., 2005; Diamond et al., 2018; Grasby et al., 2016; Pastorelli et al., 2001; Pfeifer et al., 1992; Reyes et al., 2010; Sonney & Vuataz, 2009; Stober, 1995; Stober & Bucher, 2015; Stober et al., 1999, 2016; Taillefer et al., 2018; Wanner et al., 2020). Upwelling water may or may not contain a foreign water component of unknown origin and composition depending on the local flow field (Wanner et al., 2020).

The flow velocity of < 2 m $year^{-1}$ derived from numerical models of fluid flow through the bedrock of rugged mountains (Wanner et al., 2018) suggests that the fluid is close to ion exchange equilibrium with the fracture surfaces of the rocks at all times. Thus ion exchange during flow through bedrock fractures does not significantly modify the composition of the fluids derived from dissolution and precipitation reaction.

Water in the crystalline continental basement is mostly in contact with K-feldspar, Na-rich plagioclase (albite, oligoclase), quartz, a small modal amount of biotite and various accessory minerals. The fractures are often coated with minerals that formed from alteration reactions of water with the primary minerals of granite and gneiss. Alteration minerals include clays (e.g. chlorite, kaolinite, smectite), zeolites, carbonates, sulfates, oxides and occasionally also sulfides (Stalder et al., 1980). The local fluid is typically not in equilibrium with plagioclase and biotite (and other Fe–Mg silicates) but close to saturation with K-feldspar and quartz. With respect to secondary alteration minerals, the wide range of different waters are supersaturated with respect to a distinct assemblage of product phases of the WRI-process and

undersaturated with respect to other alternative product assemblages (Bucher & Stober, 2010). Thus characteristic alteration assemblages are present along the fractures reflecting also the distinct nature of water composition that result from the local WRI (Aquilina, Pauwels, et al., 1997; Aquilina, Sureau, et al., 1997; Grimaud et al., 1990; Pauwels et al., 1993).

Here we present and discuss the composition of 211 water samples collected in the Sedrun section in the new Gotthard Base Tunnel excavated predominantly in crystalline basement rocks. The tunnel is the key structure of the new transversal of the Alps (NEAT) and the longest tunnel in the world (57 km). The water samples were collected during drilling of the tunnel from water conducting fractures before these were permanently sealed with concrete. The water samples represent a 10 km long hydrochemical section along the tunnel axis at depths between 900 and 2350 m below surface. Without the tunnel an equivalent set of samples would have required ~ 120 deep research wells drilled to 1–2.4 km in the upper continental crust. Additionally, we report in this paper stable isotope data and some gas analyses from water inflows. The very rugged topography with up to 2350 m basement rocks above the tunnel axis results in significant Darcy-flow that removed older water components such as saline brines that normally are present in continental basement (Bucher & Stober, 2010). The presented water data illuminate the mechanisms of solute acquisition of deep basement water in the continental upper crust related to sole local water–rock-interaction.

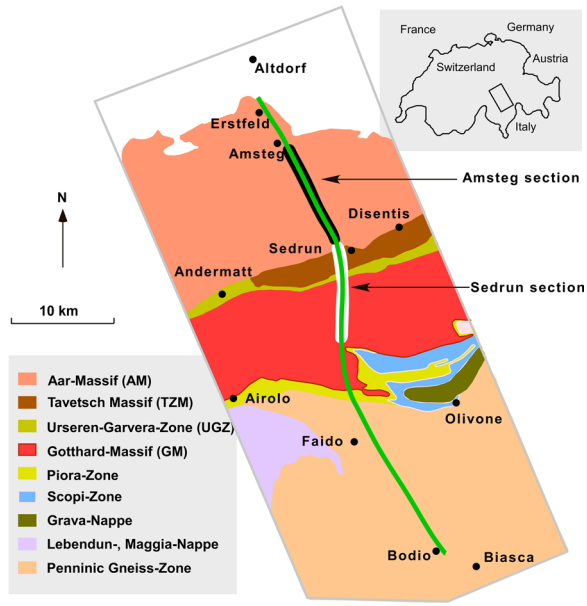

Fig. 1 Schematic geological map showing the course of the Gotthard Rail Base Tunnel. The Sedrun section is highlighted in white, the Amsteg section in black. The tunnel traverses from north to south Pre-Alpine basement of the Aar-Massif (AM), the Tavetsch Intermediate Massif (Tavetscher Zwischenmassiv, TZM), the Gotthard-Massif (GM), and the Penninic Gneiss-Zone. These basement units are separated by in part young-Paleozoic and Mesozoic sedimentary units of the Clavaniev-Zone (CZ), the Urseren-Garvera-Zone (UGZ), and the Piora-Zone. Tertiary Alpine orogeny deformed the Pre-Alpine basement and N-S compression resulted in steeply dipping units (Fig. 2) and E-W trending foliation (Steck & Hunziker, 1994)

2 The Gotthard Base Tunnel along the Sedrun section

The Gotthard Base Tunnel (GBT) in central Switzerland crosses the Alps between Erstfeld and Bodio at about 500 m above sea level (a.s.l.). It is with 57 km the longest tunnel in the world (Fig. 1). The total length of drilled tunnels, shafts and passages is 152 km. Drilling started in 1999 and the tunnel opened for regular service in 2016. It is part of the new railway link (NEAT) providing a connection between central and southern Europe. The link consists of two single-track rail tunnels connected by passages at regular intervals.

Tunnel construction was divided into five sections, which were excavated separately. This study relates to the Sedrun section in the central part of the tunnel (Fig. 1). The section is named after the village of Sedrun in the Rhine river valley at an elevation of 1334 m. Access to the base level of 500 m of the tunnel was provided by a vertical shaft > 800 m deep. The presented data include waters from the southernmost Amsteg section (Figs. 1, 2). The hydrochemical properties of fracture water along Amsteg section can be found in Seelig and Bucher (2010), Bucher et al. (2012), and Wanner et al. (2020).

The village of Sedrun lies in Val Tujetsch, a deep valley formed by the Anterior Rhine (Fig. 1). The valley follows the geological unit TZM-north (Tavetscher Zwischenmassiv), consisting of nearly vertical dipping heavily sheared and fractured rocks (Fig. 2). The Gotthard Base Tunnel passes through this zone about 800 m beneath Sedrun. Due to the special local conditions access and preparatory works for the Sedrun section already started in 1996 and lasted until 2002. Actual tunneling work at the level of the Gotthard Base Tunnel began at this location in 2003/2004 with two tunnels in northern and two in southern direction. The tunnels driven in the Sedrun section extend from north to south along a distance of 8569 m in the eastern single-track tunnel and 8735 m in the western tunnel. The highest point of the Gotthard Base Tunnel is located in the Sedrun section at km 21.733 at an elevation of 549 m. All positions and sites in the tunnel are given as km from the north portal near Erstfeld (Fig. 1). All four main tunnels were drilled

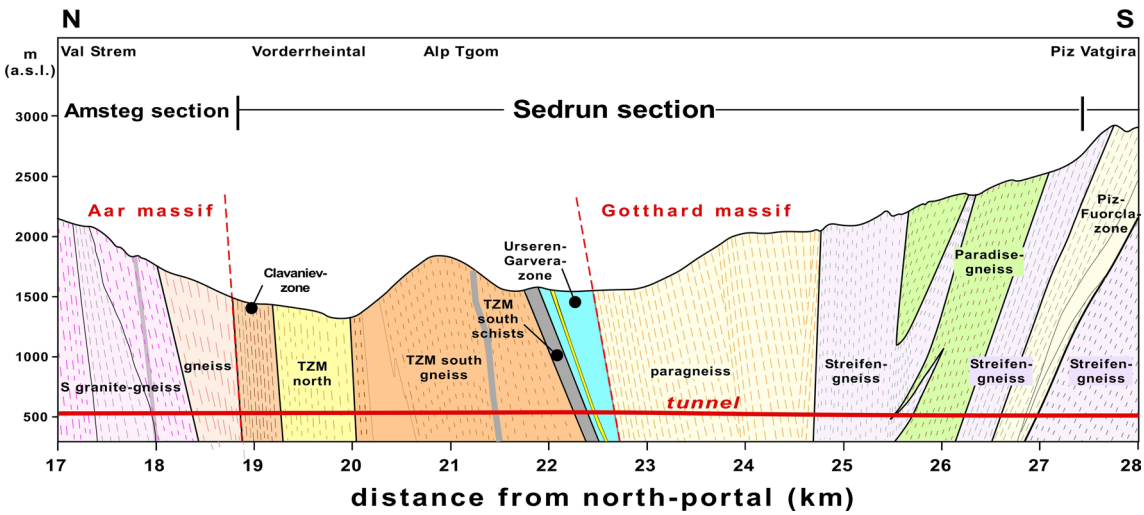

Fig. 2 Geological cross section along the investigated tunnel section Sedrun. Triassic Röti dolomite marble of the Urseren-Garvera Zone (UGZ) highlighted in yellow

downwards from the crest point. Maximum overburden was about 900 m at tunnel level in the north tunnel drives and the highest overburden in the southern tunnel of the Sedrun section is about 2350 m close to Piz Vatgira (2983 m) above the tunnel. The north drives were completed with the breakthrough to the Amsteg section in 2007 and the south drives in 2010 with the opening for the TBM (tunnel boring machine) arriving from Faido in the south (Fig. 1). All tunnels, shafts and passages in the Sedrun section were excavated conventionally by drill and blast (Gruber & Holstein, 2016).

3 Geological outline of the Sedrun section

The Gotthard tunnel traverses from north to south alpine overprinted Pre-Alpine basement of the Aar Massif (AM), the Tavetsch Intermediate Massif (Tavetscher Zwischenmassiv, TZM), the Gotthard-Massif (GM), and the Penninic Gneiss Nappes (Fig. 1). The continental basement units are separated by late-Paleozoic and Mesozoic meta-sedimentary cover units. Alpine orogeny in the Tertiary deformed the Pre-Alpine basement and N-S compression resulted in steeply dipping units in the northern sections including the Sedrun section (Fig. 2) and E-W trending foliation (Guntli et al., 2016; Steck & Hunziker, 1994). The different rock units traversed by the tunnel are briefly presented from north to south.

The northernmost water and rock samples of this study were collected (strictly in the Amsteg section) in pre-Variscan gneisses of the southern Aar Massif, a NE-SW trending complex of crystalline basement overprinted by Alpine metamorphism and deformation. The tunnel in the southern part of the Amsteg section crosses steeply dipping slabs of gneiss and schist and the predominant nearly vertical fracture system at high angles (Fig. 2). The rocks contain quartz, K-feldspar, Na-feldspar (albite, plagioclase) and chlorite. Common minor minerals include muscovite and biotite, with variable degrees of chloritization. Chlorite is the dominant clay mineral that occurs in large amounts as chlorite sand in the fissures. Open fractures and fissures frequently contain late Ca–zeolites, including predominant laumontite and very late stilbite formed by precipitation from infiltrating water at low temperature (Bucher & Weisenberger, 2013; Weisenberger & Bucher, 2010). Apophyllite occurring together with laumontite in fissures formed about 2 Ma ago at a temperature of 68 °C and a position about 500 m below the present tunnel level (Weisenberger et al., 2012). The present tunnel temperature in the southern gneiss of the Aar massif is about 38–40 °C (Fig. 3).

The Clavaniev-Zone (CZ) is the strongly fractured and sheared unit between the Aar Massif and the basement unit in the south (TZM, see below. The Clavaniev-Zone is mainly composed of Cal- and Chl-bearing two-mica schist and gneiss and of Bt- and Chl-schists (abbreviations of mineral names from Whitney & Evans, 2010). Leucocratic mica-poor gneisses occur as well. The CZ is the intensively sheared and strongly deformed contact unit to the Tavetsch Massif in the south. Over 95% of the rocks in the CZ may be designated as cataclasites or cataclastic fault rocks. However, the degree of late brittle deformation varies considerably (Guntli et al., 2016; Leu & Wyss, 1992; Mezger et al., 2013). The rocks of the CZ are probably of Permo-Carboniferous age (Guntli et al., 2016).

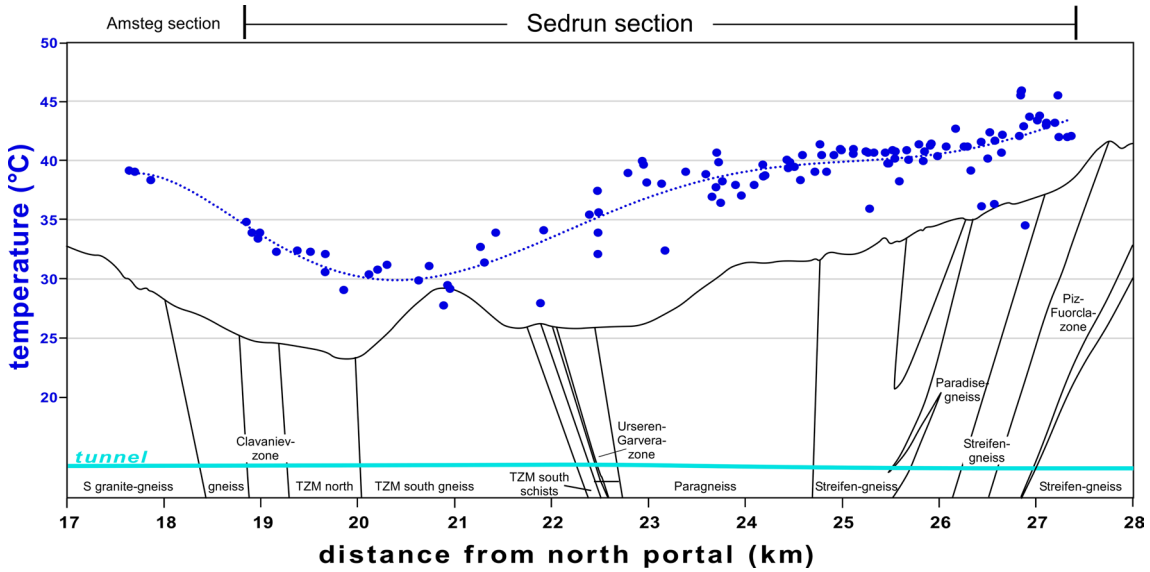

Fig. 3 Water temperature measured in the tunnel. Dotted line: Model temperature fitted to measured data

The Intermediate Massif of Tavetsch (TZM, Tavetscher-Zwischenmassiv) is a smaller basement unit between the Aar Massif in the north and the Gotthard Massif in the south. The unit can be subdivided into a deformed gneiss section (TZM-north) and a schist and gneiss section (TZM-south) with a lower degree of Alpine overprint. The conditions for tunnel construction in TZM-south with its intact pre-Variscan gneiss, schist, pegmatite and meta-pyroclastic rock were significantly better than in TZM-north (Guntli, 2005; Guntli et al., 2016; Loew et al., 2010). An approximately 20 m thick very strongly cataclastically overprinted mica-schist occurs in an extended fault zone of the southern part of TZM-north (Guntli, 2005). The main lithological components of TZM are: (i) In TZM-north two-mica-gneisses and –schists, Bt-bearing Chl-Ms-schists and –gneisses with sporadic lenses of ultrabasic rocks and amphibolite. TZM-north is strongly reworked during Alpine ductile deformation and subsequent brittle faulting. (ii) The TZM-south-gneiss includes Bt-Ms-gneiss, Ms-gneiss, Grt-amphibolite and irregular ultrabasic lenses and pegmatites. (iii) TZM-south-schists include Cal-bearing Ms-Chl schists with similarity to the Permo-Carboniferous schists of the UGZ.

The Urseren Garvera Zone (UGZ) (Fig. 2) is a thin unit of meta-sediments between the basement massifs of Tavetsch (TZM) and Gotthard (GM). The sedimentary sequence represents the cover unit of the TZM basement and includes from oldest to youngest (Guntli, 2005; Loew et al., 2010): (i) Permo-Carboniferous: Cal-bearing Ms-schists and phyllites; (ii) Triassic Röti formation: Hem-bearing dolomite marbles with phyllite layers (highlighted in yellow on Fig. 2); (iii) Triassic Quarten formation: Chl-Ms-schists and -phyllites; (iv) Liassic Prodkamm formation: dark gray to black graphitic schists, locally also Cal-bearing; (v) Liassic Spitzmeilen formation: Qz-rich dolomite marbles and quartzites. The UGZ was drilled from N to S and a tectonic repetition of the Triassic Röti-formation and parts of the Permian-Carboniferous sediments was observed.

The Gotthard Massif (GM) is a major basement unit of the Central Alps and is traversed by the Sedrun section of the tunnel at a length of about 4650 m (Fig. 2). It continues to further south in the Faido section of the Gotthard-tunnel. The major units of the predominantly pre-Variscan GM in the Sedrun section: (i) Paragneiss unit; (ii) Streifen-gneiss-north; (iii) Paradise-gneiss; (iv) Streifen-gneiss-south; (v) Piz-Fuorcla-Zone; and again (vi) Streifen-gneiss-south (s.s). Along the northern contact to the UGZ the GM consists of a thin zone with chlorite-sericite-schists (14 m, both tubes). The GM is transected by steeply dipping brittle and brittle-ductile faults (Fig. 2).

The main units of the GM can be petrographically characterized as follows: (i) The very heterogeneous Paragneiss unit consists predominantly of Bt-Ms-gneiss with large modal variations of mica. Other rock types present in the unit include Bt-gneiss, Bt-Chl-Ms schist, Grt-amphibolite, and lenses of ultramafic rocks. Also lenses of calcsilicate rocks containing Ep and Grt occur in the gneiss. (ii) Streifen-gneiss-north is a unit of heterogeneous pre-Variscan migmatites. Predominant is leucocratic

Bt-Ms Kfs-gneiss. (iii) Paradise-gneiss is a characteristic dark Chl- and Bt-rich Pl-gneiss with abundant calcsilicate lenses. It grades into Ms-bearing gneiss towards south containing lenses of Grt-amphibolite and ultramafic rocks. (iv) The Streifen-gneiss-south unit is an Ordovician granite deformed during Variscan and Alpine orogeny. It is a leucocratic two-mica granite-gneiss crosscut by numerous meta-lamprophyre dikes. (v) The Piz-Fuorcla-Zone consists predominantly of dark migmatitic Chl-Bt-Ms Pl-gneiss. Locally the unit also contains Chl-Ms schists and Grt-bearing amphibolite.

The intensity of Alpine metamorphism increases from north to south. Peak temperature along the Sedrun section of the tunnel increases from greenschist facies in the Aar Massif (about 400 °C at Chrüzlistock) to beginning amphibolite facies in the Gotthard-Massif (about 500 °C at Piz Vatgira) (Frey et al., 1980). Alpine tectonic deformation changes from predominantly brittle to ductile along the Sedrun section. However, the water conducting features such as fractures, faults and other brittle deformation structures were created during late uplift and cooling of the basement units.

Secondary clays, specifically illite, smectite and rarely also kaolinite typical of near surface alteration of metagranitic rocks have been found in clayey mud from basement units of the Sedrun section (Guntli, 2005).

Sheared surfaces are coated with graphite, up to 5% of rock. Late fractures often contain calcite. Also chlorite seals late fractures. Muscovite is present in most gneisses, also as late mineral in fractures and veins. Strong sericitization of K-feldspar is distinct in most samples.

4 Methods

The team of NEAT geologists, the Swiss analytical laboratory Bachema AG, and the Institute of Mineralogy, Petrology and Geochemistry (IMPG) of the University of Freiburg collected water and rock samples during tunnel driving between January 2003 and October 2010 (Guntli et al., 2016). The samples were taken from open fractures/fault zones and small-diameter, shallow exploration wells in both pipes of the tunnel. The location of water samples in the tunnels (Additional file 1: Table S1) is reported as 'tunnel meter (TM)', given in kilometers from the N-portal near Erstfeld (Fig. 1). The location of the samples from the two parallel tunnel-pipes are normalized and projected onto each other along strike of the geological units. The first northernmost sample has been taken at tunnel km 17.627, the last one in the south at km 27.339 km. Thus, we present water samples from a section of about 10 km length in the tunnel.

Temperature and electrical conductivity were always measured in situ during sampling in the tunnel. The collected water samples were analyzed in the laboratories of Bachema AG and of IMPG. Since it was not often possible to measure pH directly in the tunnel, most pH-values were analyzed in the two labs, in the Bachema-lab with a minimum time-delay and in the IMPG-lab sometimes with larger delay depending on who collected the samples (NEAT team or IMPG). In total we present 211 water analyses, 80 analyzed by Bachema and 131 by IMPG, 11 water samples were analyzed in both labs. A few water samples were analyzed for dissolved H_2S and CH_4 at IMPG. The redox potential was not consistently measured at the inflows. Later measurements in the laboratories after various irregular storage times do not reliably reflect the redox state of the samples. Thus we do not discuss redox potentials in this communication.

Furthermore, it was possible collecting water samples as time series at some distinct inflow points in the tunnel. The data permitted an analysis of the effect of changing hydraulic conditions caused by the excavation of the tunnel on the hydrochemistry. All in all we present water analyses from 119 different inflow points of the Sedrun tunnel section. The opportunity for collecting this unique data set was made possible by NEAT. The water inflow points cannot be resampled today because of the massive final concrete-lined tubes.

At the IMPG-lab all anions and the monovalent cations were measured with a DX-120 ion chromatograph (IC) from Dionex. Other cations were analyzed with atomic absorption spectrometry (Vario 6 from Analytik Jena). Silica and boron were determined using photometry (UV/VIS spectrometer Lambda 40 from PerkinElmer). Analyses in the Bachema-lab were carried out with similar methods, i.e. by using ion chromatography and photometry. The carbonate species were determined with acid titration in both laboratories. Analyses were controlled by comparison with the measured electrical conductivity and by the calculated electrical neutrality. The sum of the carbonate species is reported as Total Inorganic Carbon (TIC).

Generally, the analytical data produced by Bachema and IMPG showed very small differences, except for samples that were analyzed after long storage periods, i.e. water samples collected by the NEAT Team and later analyzed at IMPG in Freiburg. These samples showed lower pH-values with correspondingly altered CO_3- and HCO_3-concentrations compared to fresh samples. The pH decrease after long storage periods of the water is due to diffusion of atmospheric CO_2 into the PVC-bottles (Wanner et al., 2020). Some samples have been stored in PVC-bottles in Sedrun for some weeks or month before being analyzed at IMPG. Samples measured directly at the inflow point in the tunnel and immediately afterwards in the laboratory (the same or following day) showed identical pH values.

The code PHREEQC version 2.14 (Parkhurst & Appelo, 1999) was used for computing the distribution of species, species activities, mass transfers and saturation states from the database LLNL.dat (Wolery, 1992).

5 Results: composition of Gotthard tunnel water

Water and rock temperature directly correlates with the rock column above the tunnel floor and reflects topography (Fig. 3). However, a probably existing 3D-effect of the topography on temperature is not visibly reflected by the data along the 2D-section. Enhanced discharge rates, especially in the tunnel segments 22.9–23.7, 24.7–25.0 and 26.8–27.2 km, do not noticeably affect the water temperature. Discharge does not correlate with higher or lower water temperature. At inflows with time-series data temperature decreases with time.

The pH of water shown on Fig. 4 was immediately measured at the inflow, ignoring data determined after longer storage periods. A very prominent feature of the waters is their generally very high pH (up to pH = 11), with a majority ranging from 8.9 to 10.5. There are two tunnel segments with significantly lower pH (Fig. 4). The lowest values (pH 7.9–8.4) were measured in waters from the southernmost TZM-south gneiss and TZM-south schists and in the UGZ (Urseren Garvera Zone) (21.868–22.659 km). Water from the fault zone between UGZ and GM had a pH of 7.9. The considerably lower pH is associated with Ca-carbonate and Ca-sulfate waters. There is a noticeable low pH zone (pH 8.2–9.3) associated with Paradise-gneiss (25.884–26.268 km) (Fig. 4), discharging Na-carbonate water. At the inflows sampled over longer periods of time pH-values decreased with time.

The total of dissolved solids (TDS) varies between 114 and 3674 mg L^{-1}. However TDS of most waters is below 500 mg L^{-1} (Fig. 5). The lowest TDS (114–371 mg L^{-1}) were measured in the gneisses of the Gotthard-Massif (GM) (> 22.7 km) with a general decrease of TDS from N to S. TDS in the GM is significantly lower than in the Aar Massif (< 18.9 km) (Bucher et al., 2012). Prominent TDS peaks are linked to a zone in the southern part of TZM-north (≤ 2162 mg L^{-1}, 19.648 km) and to the fault zone between UGZ and GM (3674 mg L^{-1}, 22.659 km) (Fig. 5). The relatively high TDS at the boundary of TZM-N and TZM-S (20 km) gradually decreases towards S (Fig. 5). It is evident that pH and TDS do not directly correlate.

5.1 Major components

The composition of the waters is distinctly related to the type of infiltrated fractured rock and other geological features. The different geological units along the Sedrun section release characteristic water from the fracture system. The typical water observed in the different units is listed in Additional file 1: Table S1. None of the chemical parameters correlates with the height of the rock column above the tunnel. In the following we omit the charge from the ion notations in the text except in equations.

5.1.1 Cations

There are two major types of cation characteristics (% meq L^{-1} Fig. 6a): (i) Mg-poor Na-Ca water and (ii) Mg-rich Ca water. The first group rules all inflow points in basement granite and gneiss. Within this group Ca-rich water dominates the S-granite-gneiss of the Aar Massif. Further to the south, in the Clavaniev-zone (CZ), Ca decreases, and Na becomes dominant though

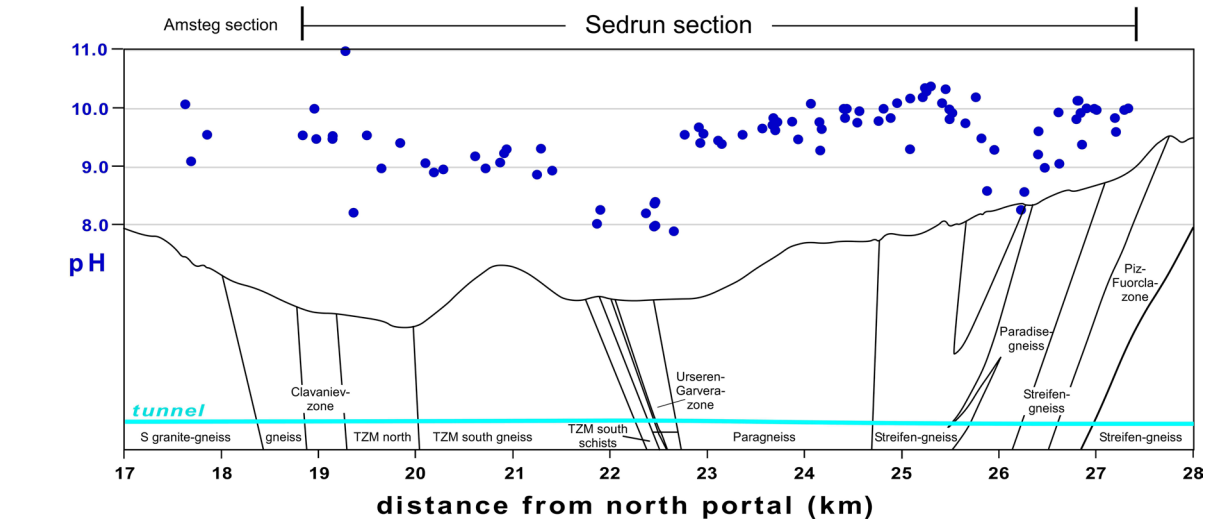

Fig. 4 pH of inflows along the tunnel-profile

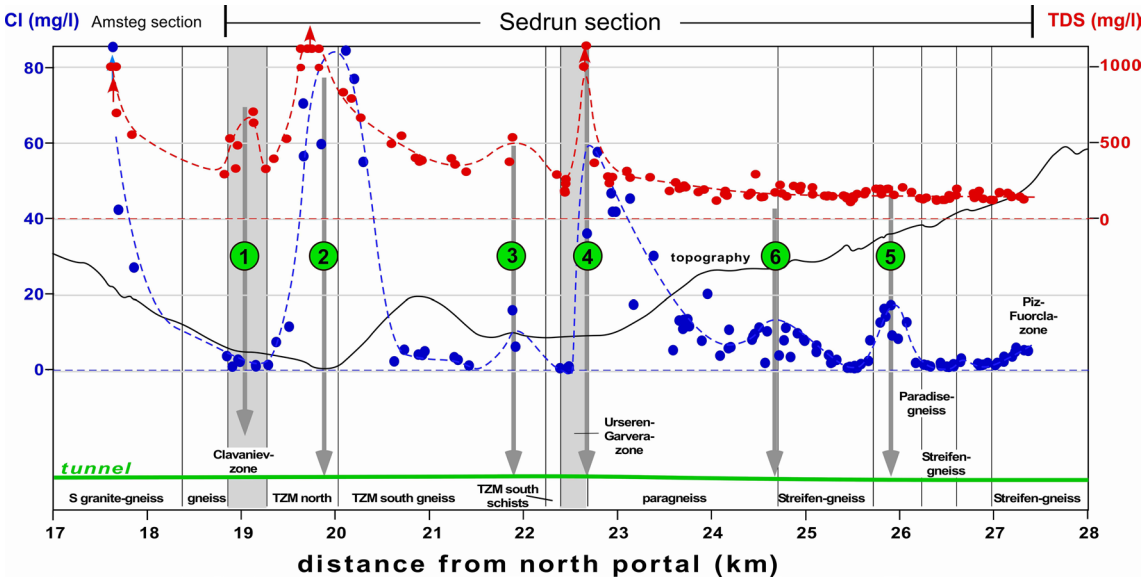

Fig. 5 Total of dissolved solids (TDS) and chloride concentration of inflows. Numbers 1–6 in green circles: strongly fractured zones with high discharge rates, high TDS and Cl (see discussion Sect. 7)

Ca-concentration remains high. In the TZM-north the collected waters contain predominantly Na and Ca is very low. In contrast TZM-south released Na-rich water with distinctly higher Ca. The water from the GM contains predominantly Na, in many inflows Na is essentially the only major cation present. A few GM waters from Streifen-gneiss south contain relatively high Ca. The second group of Mg-rich Ca-water is related to the metasediment zone UGZ between TZM and GM.

Sodium is the prime cation in most waters (% meq L^{-1} Fig. 6a). It varies in concentration by a factor of about up to 50 and reaches a maximum of 670 mg L^{-1}, but is typically below 200 mg L^{-1} (mg L^{-1} Fig. 7). Along the Sedrun section Na shows two distinct maxima. They are at the same inflows where TDS is very high (Fig. 5): at the boundary of TZM-north ($\leq$673.0 mg L^{-1}, 19.648 km) and TZM-south ($\leq$263.0 mg L^{-1}, 20.188 km), and the fault zone between UGZ and GM (638.0 mg L^{-1}, 22.659 km). In the Gotthard Massif (GM) Na is the dominant cation, however, low in concentration.

Calcium is generally very low (Fig. 7) typically below 10 mg L^{-1} but reaches a maximum of 426 mg L^{-1} in the fault zone between UGZ and GM at 22.659 km. Relatively high Ca-concentration was measured in the Aar Massif (up to 333 mg L^{-1} at 17.627 km). Elevated concentrations occur also in the Clavaniev-Zone (62.6 mg L^{-1} at 19.143 km), the southern TZM-south schists (56.8 mg L^{-1} at 21.868 km), and in an inflow within the Paragneiss of the GM (25.3 mg L^{-1}, 24.486 km). Ca is the dominant cation in the UGZ, where calcite- and dolomite marble are prominent rocks, and in the Aar Massif (% meq L^{-1} Fig. 6a). In the TZM south calcite-bearing schists at km 21.868 produce Ca-rich water.

The mole fraction Ca/(Ca + Na) is generally much higher in the Aar Massif (X_{Ca} = 0.2 – 0.42) than in the Gotthard-Massif (mean X_{Ca} = 0.033). Increased $X_{Ca} > 0.1$ are observed in the southern CZ (19.143–19.276 km) and in the TZM-south-schists and the UGZ (21.868–22.659 km). The presence of dolomite-calcite marbles in the UGZ and of calcite in TZM-south schists results in high X_{Ca} of the inflows in these units. Slightly increased $X_{Ca} > 0.1$ was also observed at various locations in the GM (24.486, 25.422, 26.268–26.498 km).

Magnesium is typically below 3 mg L^{-1} with the exception of the Urseren-Garvera-zone (UGZ) where the inflows are also rich in Ca (% meq L^{-1} Fig. 6a). The dolomite marbles of the UGZ produce Mg concentrations of up to 38 mg L^{-1}. Relatively high Mg-concentrations were also observed in the southern TZM-south (11.7 mg L^{-1}, 21.868 km) where Ca is elevated (56.8 mg L^{-1}) (Fig. 7).

Potassium is normally below 3 mg L^{-1}. Increased K occurs in inflows in the fault zone between UGZ and GM (K = 12.1 mg L^{-1}) and in the southern TZM-north with a maximum of 12.0 mg L^{-1} at 19.648 km. Potassium was not analyzed in tunnel segment 19.9–22.3 km, i.e. in the TZM-south gneiss.

5.1.2 Anions

The dominant anions (% meq L^{-1} Fig. 6b) are the carbonates HCO_3 and CO_3 (HCO_3 at pH < 10.33) closely

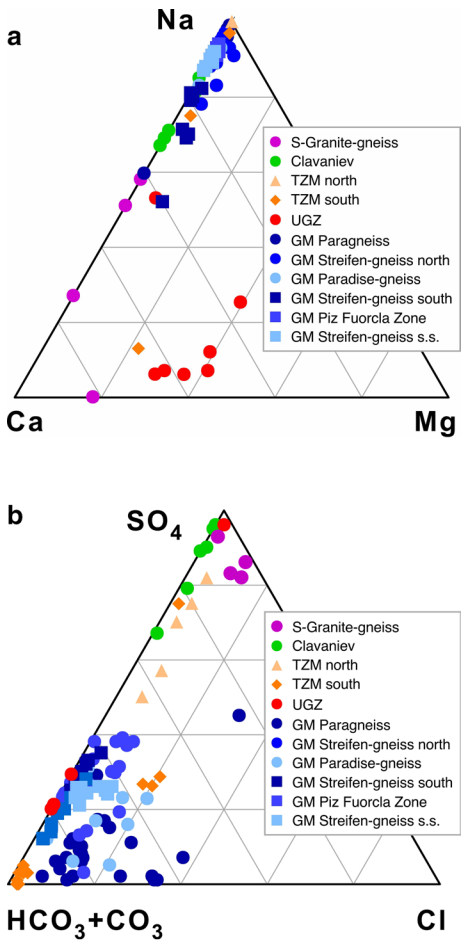

Fig. 6 Major ion concentrations in tunnel inflows shown in % meq L^{-1}: **a** cations; **b** anions

representing together the Total of Inorganic Carbon (TIC). Water from the S-granite-gneiss of the Aar Massif, the Clavaniev-zone, and TZM-north contain high sulfate (SO_4) concentrations. Also Paragneiss water from the GM contains predominantly SO_4. Cl is present in concentrations of up to 40% meq L^{-1} of the anions predominantly in the rocks from the GM. Especially waters from the GM Paragneiss are characterized by high Cl-concentrations. Water from the TZM-south and GM Paragneiss contain up to 20% meq L^{-1} chloride (Fig. 6b).

Chloride: The tunnel-waters contain typically much higher molar Na than Cl. In the Aar Massif Cl-concentrations with up to 93.1 mg L^{-1} are significantly higher on average than in the GM (max. Cl = 60 mg L^{-1}). A strong correlation between sodium and chloride was not detectable, even though elevated chloride concentrations were observed at the same sites in the tunnel where Na was enriched: In the southern part of TZM-north ($\leq$ 70.5 mg L^{-1}, 19.648 km) together with northern part of TZM-south ($\leq$ 84.5 mg L^{-1}, 20.100 km) and the UGZ and the northern Paragneiss of GM ($\leq$ 57.6 mg L^{-1}, 22.770 km) (Fig. 5).

A distinct and prominent Cl-peak is located between the GM Streifen-gneiss and Paradise-gneiss at tunnel km 25.8 (Fig. 5). It coincides with a very small peak in Na-concentration (Fig. 7) at the same location. However, the sites with enhanced Cl-concentration do not show low Na/Cl-ratios. Molar Na/Cl is typically much higher than 10 and can be as high as 250. A possible correlation between high Cl-concentrations and enhanced temperatures resulting from upwelling of deep waters is not shown by the data apart from an area at kilometer 23.0 km (Figs. 3, 5). However, some waters in the GM

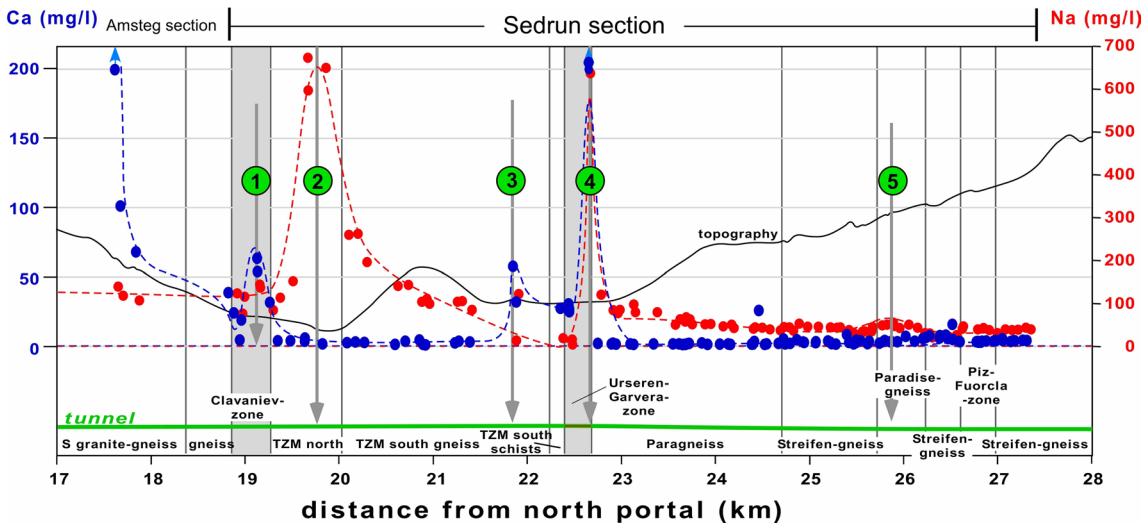

Fig. 7 Ca and Na concentration along the Sedrun Section: Numbers 1–6 in green circles: Strongly fractured zones with high discharge rates, high TDS and Cl (see discussion Sect. 7)

with enhanced Cl-concentrations are slightly oversaturated with respect to quartz (SI_{Qz}: 0.29–0.64), potentially indicating upwelling of waters from areas with higher temperature and salinity: 22.916–23.365, 23.938, 24.486, 25.863, 27.211–27.339 km.

Sulfate (SO_4) generally decreases southwards (Additional file 1: Table S1). Sulfate concentration is exceptionally high in the TZM-north (1133 mg L^{-1} at 19.650 km) and in the fault zone between UGZ and GM at 22.669 km with 2440 mg L^{-1}. Samples from the Aar Massif and the Clavaniev-zone showed also relatively high SO_4-concentrations (>400 mg L^{-1}) (in % meq L^{-1} Fig. 6b). In the TZM-south gneiss SO_4 was generally lower than in TZM-north. However, in the northern part of TZM-south SO_4 was higher (≤158 mg L^{-1}) than in the central part (<9 mgL^{-1}) followed by again higher values in the southernmost part (≤265 mg L^{-1}). Sulfate in the GM is relatively low (≤43 mg L^{-1}), significantly lower than in the Aar Massif. Slightly increased SO_4-concentrations occur in the GM Streifen-gneiss-north of the GM at tunnel-km ± 25.0 km (≤43 mg L^{-1}).

Ca and SO_4 do not correlate and Ca/SO_4 was < 1 (mole ratio) in most samples from the GM. Enhanced Ca/SO_4-values (>1) are preferentially observed in the UGZ and slightly increased values at some localities of the TZM-south. In the Dol- and Cal-bearing rocks of the UGZ increased Ca in water (Fig. 7) leads to $Ca/SO_4 > 1$.

The SO_4/Cl-ratio (in meq L^{-1}) varies over several orders of magnitude. SO_4/Cl can be specifically related to location and rock type: the Clavaniev-Zone (up to 85) and the UGZ (up to 25). There are two locations in the GM (km: 25.4; 26.3) with relatively high yet less extreme SO_4/Cl-ratios.

5.2 Minor components

Bromide (Br) concentration was generally very low (<1.1 mg L^{-1}). All data were produced by IMPG. Thus Br-concentration data are lacking for some localities, especially from TZM-south. Within the GM Br decreases in southern direction. However, the measured Cl/Br mass ratio for the entire section is < 120. Thus Cl/Br is typical of crystalline basement rocks. It is much lower than that of seawater (Cl/Br = 288) (Stober & Bucher, 1999) and far below Cl/Br from evaporite water. The mean value in the GM is Cl/Br = 60, which is even lower than in the Aar Massif of the Amsteg section (Bucher et al., 2012). A further regional trend within the tunnel section is not detectable.

The concentration of fluoride (F) is relatively high in most water samples. In many samples F is a major anion. The highest value (15.4 mg L^{-1}) was detected at 19.550 km in the TZM-north. The unit showed generally high F-concentrations. In TZM-south no F was analyzed. The UGZ showed very low F-concentrations (<1.0 mg L^{-1}). In the Aar Massif enhanced F-concentrations (≤4.19 mg L^{-1}) were measured. Several locations in the GM also showed high F-concentration. In the northern part of the GM F decreases in southern direction until tunnel km 25.5 from 7.2 mg L^{-1} to very low values of 0.2 mg L^{-1} and then, farther to the south, F increases again up to 8.1 mg L^{-1} below Piz Vatgira (Fig. 2). F does not correlate with TDS or overburden. Along the tunnel section F-concentration exceeds Cl (mass ratio) at certain locations drastically:

- -CZ: F/Cl = 2.02 at 19.143 km.
- -TZM-north: F/Cl ≤ 2.03 at 19.361–19.497 km.
- -UGZ: F/Cl ≤ 6.26.
- -GM: specific locations in the Paragneiss (24.548 km: F/Cl = 1.18) and Streifen-gneiss (25.422 km: F/Cl = 1.12 and 25.457 km: F/Cl = 1.07).
- -GM (generally > 26.146 km, southern Paradise-gneiss, Streifen-gneiss-south, Piz-Fuorcla-zone, Streifen-gneiss-south s.s.): F/Cl= 1.86–4.52.

In the GM, F and Cl correlate and define linear trend lines with different slopes: m = 0.25 for F/Cl < 1 and m = 2 for F/Cl > 1 (Fig. 8). Possible similar correlations in other units remain undetected due to lack of F data. It follow that at many inflows F is higher than Cl (red dots Fig. 8) and F represents a major anion rather than a minor component.

Strontium (Sr) is often below detection limit (0.05 mg L^{-1}) or was not analyzed. Sr shows higher concentrations at sites with elevated Ca-concentrations, e.g. in the UGZ with a significant peak of 11.3 mg L^{-1} in the fault zone

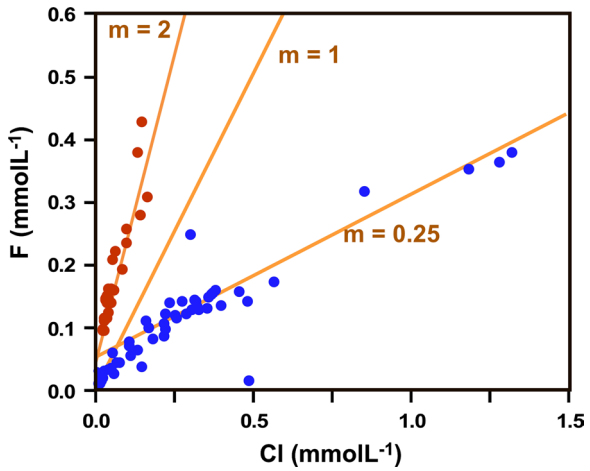

Fig. 8 Chloride vs. fluoride concentration in mmol L^{-1}. Samples with F > Cl in red, samples with F < Cl as blue dots. All samples from the Gotthad Massif (GM). m = slope of reference lines

between UGZ and GM (22.659 km). However, only a week correlation between Ca and Sr was detectable.

Iron (Fe) is with a mean of 0.15 mg L^{-1} relatively high but the reported value includes colloidal Fe. Besides Fe was not always measured or was below detection limit (0.02 mg L^{-1}).

5.3 Silica

Dissolved silica, expressed as SiO_2, reached concentrations of up to 58 mg L^{-1} in the GM Streifen-gneiss. Silica in solution increases with temperature and with pH for pH > 8.0. Silica in solution strongly correlates with pH (Fig. 9) and its concentration drastically increases at high pH. Figure 9 shows exclusively data from waters with pH-values measured at the sampling site ignoring all samples where pH was measured after extended storage times (see above). Measured water temperatures in the tunnel range from 35 to 45 °C (Fig. 3). Most water samples are close to equilibrium with quartz or slightly supersaturated with respect to quartz (Fig. 9). Possible upwelling waters in the tunnel with a higher silica-signature and the variation in tunnel-temperature may cause some scatter in the data shown in Fig. 9. Dissolved silica is typically in the range of 20–30% of TDS (mg L^{-1}) in gneiss of the GM, with the exception of the Paradise-gneiss unit where it is markedly lower (about 10%).

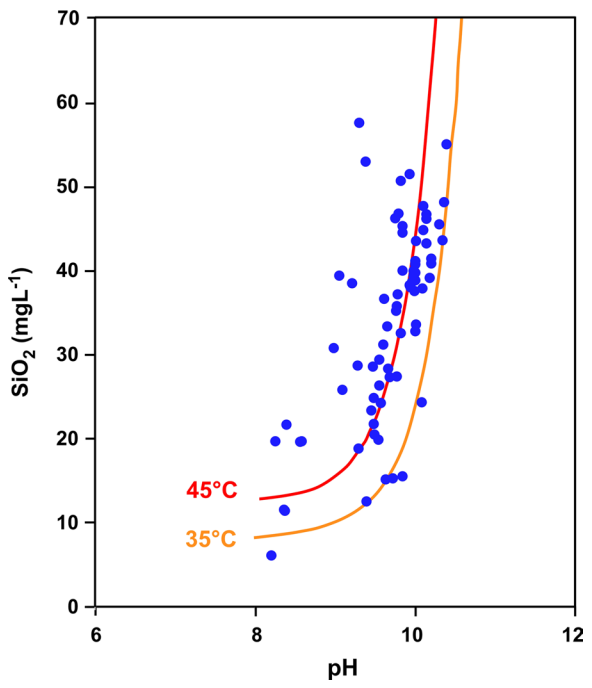

Fig. 9 Dissolved aqueous silica in mg L^{-1} vs. pH. Computed saturation with respect to quartz at 35 °C and 45 °C from PHREEQC (Parkhurst & Appelo, 1999)

5.4 Saturation states

All water samples are strongly oversaturated with respect to Fe-oxides, goethite and hematite, indicating potential precipitation of Fe-minerals. Hematite bearing meta-arkoses are found in the UGZ. Hematite is a common and widespread and highly valued fissure mineral in the entire Sedrun region. Waters are also oversaturated with respect to dolomite and calcite, but at locations, where we could collect time series of water samples (see Sect. 6) oversaturation decreased with time. Although Ca, Mg increased with time at the Rötidolomite inflow at km 22.46 in the UGZ, SI of carbonates decreased because of decreasing temperature and HCO_3 (see Sect. 6). Generally waters are undersaturated with respect to relevant sulfate minerals such as anhydrite, gypsum, barite, and epsomite, but $SI_{sulfates}$ increases with time. Sulfide oxidation decreases with depth because dissolved atmospheric CO_2 and O_2 have been consumed at higher elevation closer to the surface. With increasing time waters with a higher sulfide oxidation capacity migrate to the tunnel level from above (see Sect. 7.3 below).

5.5 Tritium and stable isotope data

Stable isotope and tritium data were solely measured in selected water samples taken by the Bachema-lab (Guntli et al., 2016). The data represent 25 different inflow points. Generally, tritium was below detection limit (< 0.6 TU), with one exception. In the UGZ at location 22.467 km (Röti-dolomite) 1.9 ± 0.5 TU were measured. Tritium was additionally measured at three other inflow points in the UGZ, but with contents below detection limit. This implies that all tunnel waters are infiltrated the ground before 1952, apart from the water sample in the Röti-dolomite. All water samples of the time series do not show changes in tritium content. However, the time series of the water samples in the Röti-dolomite (time series > 4 years) showed small variations in tritium content, but these variations remained within the measurement accuracy of ± 0.5 TU.

The concentrations of the stable isotopes ^2H and ^{18}O are presented as δ^2H and $\delta^{18}O$ values, which represent the per mil deviation of the $^2H/^1H$ and $^{18}O/^{16}O$ ratios in the samples from those in Standard Mean Ocean Water (SMOW). Isotope ratios in atmospheric precipitation vary with climate, altitude, and location. Thus, differences in the δ^2H and $\delta^{18}O$ values of groundwater can indicate changing climate in the recharge area, or changing locations or elevation of the recharge area, due to the mass dependent fractionation of hydrogen and oxygen (Pearson et al., 1991). The global Meteoric Water Line (GMWL) describes the global annual average relationship between δ^2H and $\delta^{18}O$ (Craig, 1961). Local meteoric

water lines (LMWL) can differ from the GMWL in slope and intercept due to local effects on the fractionation of hydrogen and oxygen.

Figure 10 shows the isotopic signature of the water samples from CZ, UGZ, and GM. Tunnel waters in the Aar Massif of the Amsteg-section show similar results (Wanner et al., 2020). Most data in Fig. 10 plot along a parallel line above the GMWL. The vertical shift of the LMWL is in the order of $\delta^2H = 3$ ‰ (black arrow in Fig. 10). The most probable cause for the shift is the influence of glaciers, present during the little ice age in the area (Dietermann, 2010; Guntli et al., 2016; O'Neil, 1968; Stichler et al., 2001). Guntli et al. (2016) concluded that a verifiable influence of changing elevation of the recharge area cannot be deduced from the stable isotope data. Tunnel-waters with lower overburden (no glaciation in the little ice age) lie close to the GMWL, like samples in the Röti-dolomite (22.460 km) in the Urseren-Garvera-Zone (UGZ) and the samples in the Clavaniev-zone (Fig. 10).

The time series of water samples (see Sect. 6 below) taken in the Paragneiss of the Gotthard-Massif (23.676 km) do not show a systematic trend but solely a scatter of isotope data probably due to accuracy of determination. On the other hand the time series in the Röti-dolomite (22.467 km) of the UGZ seem to show a trend to slightly higher δ^2H and $\delta^{18}O$ values with time (green arrow on Fig. 10) possibly as a consequence of increasing temperature in the recharge area?

6 Time series of water samples

At 8 different inflow points it was possible to repeatedly collect water samples over longer periods of time. Number and duration of the time series vary between 4 and 13 samples per location and during from 4 up to 1822 days. All observation points showed changes in hydrochemistry, temperature or inflow-rate with increasing time.

The two time series of the inflow points in the UGZ (Urseren-Garvera-Zone: 22.371, 22.467) showed an increase in TDS, mainly due to increasing Ca- and SO_4-concentrations. However, Mg and Na also showed an increase with time. At observation point 22.467 (Röti formation 222.467 "Parament East") Ba increased significantly with time. In Sect. 6.1 below the main features at point 22.467 are presented in some detail.

In the Paragneiss unit of the Gotthard-Massif (GM-Paragneiss) it was possible to collect at three inflow points water samples as time series (23.636, 23.676, 23.704). At all three localities water temperature decreased with time, hydrochemistry changed and partly the inflow-rate too. Below, the main features at point 23.676 are presented in more detail (Sect. 6.2).

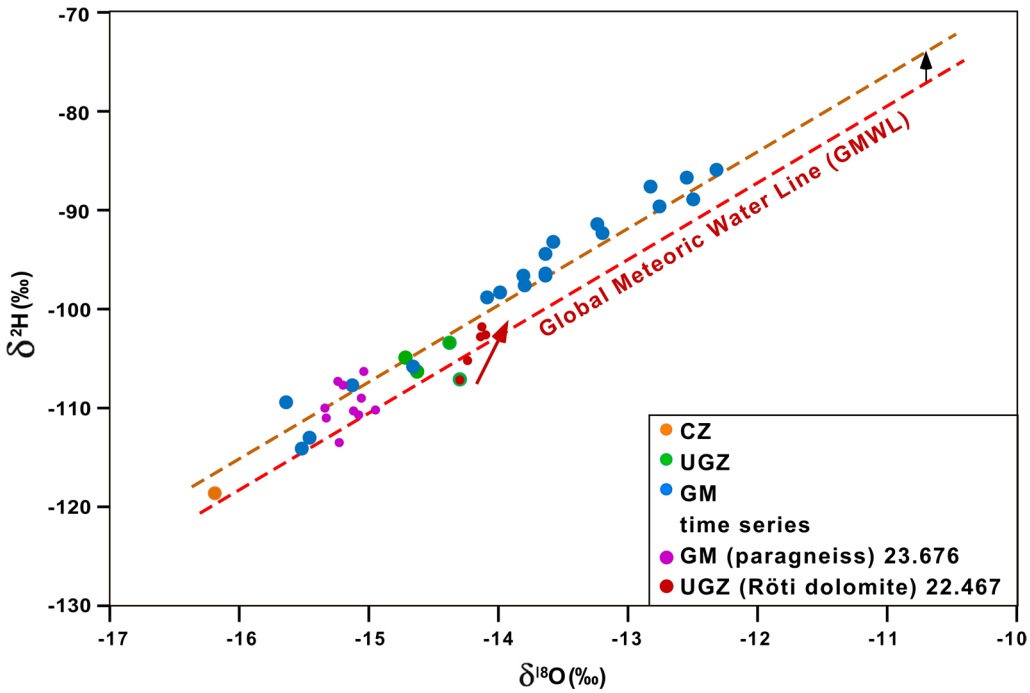

Fig. 10 Stable isotope composition of tunnel water with respect to GMWL (red). Inflow water follow a trend (orange) parallel to the GMWL with a shift of $\delta^2H = 3$ ‰ (black arrow). Also shown are the time series in the GM-Paragneiss (TM = 23.676 km) and Röti-dolomite of the UGZ (TM = 22.460 km) marked with red arrow. Accuracy of determination: $\delta^{18}O \pm 0.25$ ‰, $\delta^2H \pm 1.5$ ‰

The two time series collected in Streifen-gneiss-north of the Gotthard-Massif (km: 24.817, 24.959) showed decreasing water temperature with time. At km 24.817 also TDS, Na, and SO_4 decreased. In contrast at inflow point 26.804 in the Piz Fuorcla-Zone (GM) the water temperature increased, but TDS (including Na, SO_4, Cl) slightly decreased.

6.1 Location km 22.46 in Röti-Dolomite of the Urseren-Garvera-Zone (UGZ)

Six water samples were collected at this site (222.467 "Parament East") between September 22nd 2006 and November 14th 2010 including two samples taken at the same day. The full analysis of the first of these samples is listed as UF 7 on Table S1. Within this period inflow increased from ~ 0.1 to 0.32 L s^{-1}, whereas temperature decreased slightly from 33.2 to 32.8 °C. pH was with 8.39 marginally higher in 2006 compared to 8.16 in 2010. TDS increased significantly from 234 to 407 mg L^{-1}. The individual water components showed a varied behavior (Fig. 11). Ca, Mg, Sr, Na, Ba, and SO_4 increased whereas HCO_3 slightly decreased with time and Cl remained constant. The water evolved from Ca-Mg-HCO_3-SO_4 to Ca-Mg-SO_4-HCO_3 dominated water (meq L^{-1} based).

6.2 Location 23.676 GM-Paragneiss in the Gotthard-Massif

In the Paragneiss of the Gotthard-Massif (location km 23.676) a massive water inflow into the tunnel stopped construction work in September 2006. A small-diameter exploration hole was subsequently drilled through the gneiss with a 1.8 m long open hole in the water conducting fracture zone. This was a unique opportunity for performing a hydraulic test making it possible to derive the hydraulic properties of this zone. The drill hole was fitted with a valve and flow was limited to a constant rate of Q = 2 L s^{-1} for a longer period of time. Then flow was stopped and the resulting pressure increase in the borehole measured. The evaluation of the hydraulic test with the Cooper and Jacob (1946) method resulted in a transmissivity of T = 6.92 10^{-6} m^2 s^{-1} (Fig. 12). A remarkably high hydraulic conductivity (k_f) of 3.84 10^{-6} m s^{-1} follows from the length of the open hole.

The fluids from this site are chemically shaped by the surrounding Paragneiss. A total of 13 water samples were collected between September 22nd 2006 and April 14th 2009. Within this period inflow dropped from initially 5 to 2 L s^{-1} and temperature from 38.5 to 37.0 °C. Parallel to the temperature decrease also silica decreased (SiO_2: 27 to 22 mg L^{-1}). pH was with 9.7 marginally higher in 2006 than in 2009 (9.4). TDS increased slightly from about 205 to 235 mg L^{-1}. However, the different dissolved components showed a somewhat dissimilar behavior (Fig. 13). Whilst Ca, Mg, Na and alkalinity (TIC) increased Cl decreased slightly. Related to decreasing pH, HCO_3 increased at the expense of CO_3. However, the water did not change its principal quality with time and

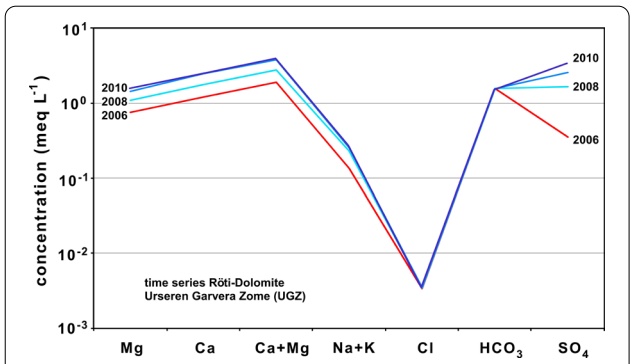

Fig. 11 Major components of water inflow (meq L^{-1}) at observation point 22.467 (Röti-dolomite in the Urseren-Garvera-Zone, UGZ) for different sampling dates (Schöller diagram): Red data from 2006, blue from 2008 to 2010. Sample UF 6 is listed in additional file 1: Table S1

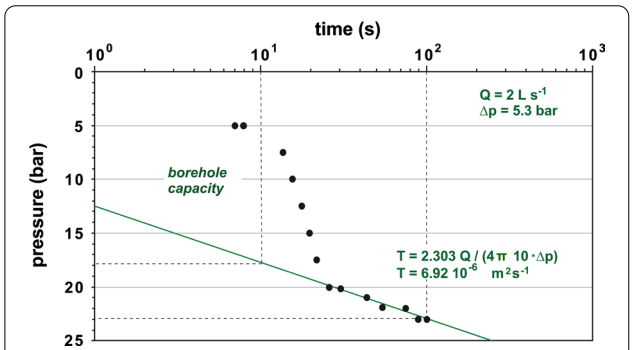

Fig. 12 Hydraulic test data and interpretation from inflow point 23.676 (Paragneiss, Gotthard Massif). Q = discharge in L s^{-1}

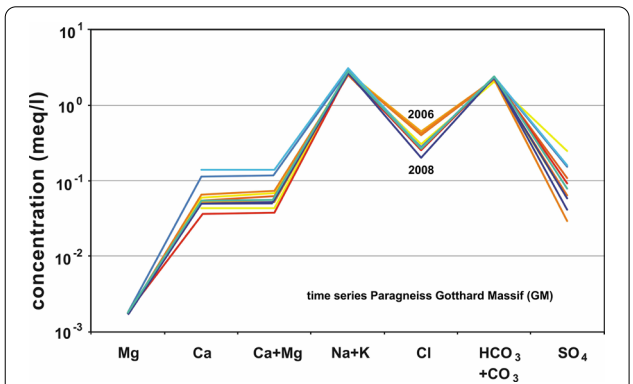

Fig. 13 Major dissolved components of water inflow (meq L^{-1}) at observation point 23.676 (Paragneiss of the Gotthard-Massif) for different sampling dates (Schöller Diagram): Yellow–red data from 2006 and 2007, blue from 2008 and 2009. Mg below detection limit = 0.02 mg L^{-1} (log meq L^{-1} = − 2.78)

remained sodium carbonate dominated (meq L^{-1} based). The computed saturation state (SI) of calcite slightly increased with time. However, the water was somewhat oversaturated with calcite from the very beginning of the time series.

7 Discussion: origin of solutes and chemical evolution of deep groundwater in continental basement

The free-flowing fracture water sampled at inflow points in the tunnel originates from meteoric water recharge at the high-alpine surface. The stable isotope composition of the water clearly indicates its meteoric origin (Fig. 10) being derived from precipitation, rain and snow, in the high-mountains above the tunnel (Fig. 14). The final composition of water at tunnel level after advection through the fracture systems of the different types of rocks must therefore be acquired from the rocks along the flow path. Dissolution of primary minerals on the fracture surfaces is the prime mechanism that increases TDS in the recharge (rain water and snowmelt) from ~ 5 mg L^{-1} to > 150 mg L^{-1} in inflows in granite and gneiss at tunnel level. The solutes are exclusively internally derived by water–rock-interaction. There is no evidence for significant modification of water composition by ion-exchange along the flow path (Wanner et al., 2018).

At a few specific inflows an additional component of upwelling waters from deeper parts below the tunnel level suggested by geochemical characteristics may occur. Upward directed flow zones have been suggested by numerical models of the flow regime along the Amsteg-section of the Aar Massif (Wanner et al., 2018). Upwelling meteoric waters indicate a long-term topography-driven flow promoted by the presence of major faults zones with elevated permeability (Diamond et al., 2018). Such flow conditions occur worldwide in rugged mountainous topography and commonly result in the occurrence of multiple hot springs (e.g. Stober et al., 2016).

Fig. 14 Streifen-gneiss mountains of the Gotthard-Massif (Piz Rondadura 3016 m). Inferred recharge area of water collected at tunnel level (500 m). Tunnel axis crosses beneath outcrops in the foreground at 2500 m (2000 m elevation difference)

7.1 Tunnel-waters with high TDS and waters in meta-sediment units

The high-TDS zones in the southern part of TZM-north and between UGZ and GM are related to strongly fractured zones and major faults (locations 1, 2, 3, 4: Fig. 5). The faults stand for enhanced reaction of the rock with descending water resulting from large rock surface area. Na and SO_4 with a relatively high Cl content dominate these waters. However, they differ with respect to Ca and Mg, which are very low in the TZM-north fracture zone. This is in contrast to the fault zone UGZ/GM (location 4; Fig. 5) and to TIC, which is higher in the TZM-north fracture zone.

Water from the Urseren-Garvera Zone contains predominantly Ca, Mg and carbonate and a fair amount of SO_4. The water results from reaction of surface water with calcite and dolomite of the UGZ marbles (reaction, rxn 1).

$$CaMg(CO_3)_2 + 2CO_2 + 2H_2O = Ca^{2+} + Mg^{2+} + 4HCO_3^- \quad (1)$$

The average UGZ water contains 1.35 mmol L^{-1} Ca and 1.10 mmol L^{-1} Mg suggesting that the water primarily reflects dolomite dissolution and only a small amount of Ca is contributed by additional calcite dissolution. Assuming recharge at T ~ 10 °C, dissolution of Dol produces 18 mg L^{-1} Ca and 11 mg L^{-1} Mg (PHREEQC), which is reasonably close to the measured average 27 mg L^{-1} Ca and 13 mg L^{-1} Mg. Calcite dissolution produces the additional Ca. The resulting model pH 8.2–8.5 closely matches the measured pH = 8.2.

Evaporitic anhydrite in the Triassic dolomite marble could contribute the observed sulfate. However, anhydrite has not been reported from the UGZ. We suggest that SO_4 originates from sulfide oxidation implied by the occurrence of pyrite-bearing graphite-schists in the UGZ (probably of Liassic age). The graphitic schists repeatedly occur along the section in the permeable Röti-formation because of Alpine shearing and folding. In a first step pyrite dissolution produces Fe(II) and bisulfide (HS^-) (rxn 2). In a second step Fe(II) is removed from the solution by precipitation of insoluble hematite containing oxidized Fe(III) (rxn 3a) and bisulfide is oxidized to sulfate (rxn 3b). The overall process (rxn 3a + rxn 3b)

produces sulfate to the solution, decreases pH and consumes oxygen dissolved in the recharge (rxn 4):

$$FeS_2 + 2H^+ = Fe^{2+} + 2HS^- \quad (2)$$

$$2Fe^{2+} + 0.5\,O_2 + 2H_2O = Fe_2O_3 + 4H^+ \quad (3a)$$

$$2HS^- + 4O_2 = 2SO_4^{2-} + 2H^+ \quad (3b)$$

$$2Fe^{2+} + 2H_2O + 4HS^- + 8.5O_2 = Fe_2O_3 + 4SO_4^{2-} + 8H^+ \quad (4)$$

The consequences of reaction 4 are evident in the tunnel where abundant red-brown stains cover the walls at some of the water discharge points. Similar processes to reaction 4 summarize the effects of acid mine drainage (e.g. Akcil & Koldas, 2006). The product phases in acid mine drainage includes jarosite, schwertmannite, goethite, and other Fe(III) minerals, most likely also present in the red crusts and stains in the open tunnel. However, hematite is the only Fe(III) mineral found in fracture cavities opened by the tunnel.

Fe(II) in solution can also be oxidized by HCO_3 to Fe(III) and precipitated as hematite (rxn 5):

$$2Fe^{2+} + 4HCO_3^- = Fe_2O_3 + 3C + CH_4 \quad (5)$$

Evidence for operation of rxn 5 is newly formed graphite and detectable methane dissolved in the water (see below) and reported graphite on fracture surfaces (Sect. 3). Reactions 1 through 5 describe the interaction of meteoric oxidized low-pH water with the carbonate minerals (here with dolomite) and pyrite of the marbles of the UGZ. Alpine rainwater has a pH of < 5.5, contains some sulfate, nitrate and has a TDS of ~ 7 mg L^{-1} or lower. The typical Cl concentration varies between 0.1 to 0.2 mg L^{-1} (rainwater data from the Täschvalley near Zermatt: Bucher et al., 2017). Rainwater in exchange equilibrium with the atmosphere contains ~ 1 mg L^{-1} TIC (0.022 mmol L^{-1}) mostly as CO_2 and 22 mg L^{-1} O_2 (0.6843 mmol L^{-1}). The reactions may co-produce graphite or amorphous carbon along with methane. Both forms of reduced carbon have been detected at water inflow points. The produced water contains the major cations Ca and Mg and the anions hydrogen-carbonate and sulfate.

The UGZ contains anhydrite and gypsum further west in the Urseren valley and the signature of sulfate dissolution has been verified in waters from the Gotthard road tunnel (Pastorelli et al., 2001). However, in the granitic and gneissic basement rocks sulfide oxydation is also the prime source of sulfate in the fracture water of the road tunnel (Pastorelli et al., 2001).

7.2 Deep water in the crystalline basement

7.2.1 Solutes

The typical basement waters of the Gotthard Massif have a TDS of 250 mg L^{-1} or lower, a high pH, and Na and carbonate as major dissolved components (Figs. 4, 5, 6, Table 2). The solutes must be generated by reaction of recharge with the crystalline basement rock matrix. The Na–K geothermometer (Stober & Bucher, 2021) produced disequilibrium temperatures of > 100 °C for many waters from the Gotthard Massif indicating that the waters are not in full exchange equilibrium with the K-feldspar + plagioclase assemblage making up the gneiss matrix. Consequently the waters are reactive and their composition is kinetically controlled. However, the reaction affinity is remarkably low for many waters implying that the distance to full equilibrium is not very large (e.g. computed T ~ 70 °C for the Kfs-Pl assemblage; 45 °C sample temperature at inflow).

Sodium has two different sources: (i) It results, together with chloride, from leaching salty fluid contained in fluid inclusion mainly in quartz, (ii) The excess sodium (Na > Cl) is contributed by dissolution of albitic plagioclase (albite and oligoclase). The hydrolysis reaction consumes protons (H^+) and thus increases pH of the water. The acidity of the reactive water originates from sulfide oxidation (in rxn 6a) and the atmospheric CO_2 in the recharge (in rxn 6b).

$$NaAlSi_3O_8 + H^+ + H_2O = Na^+ + Al(OH)_{3aq} + 3SiO_{2aq} \quad (6a)$$

$$NaAlSi_3O_8 + CO_2 + 2H_2O = Na^+ + HCO_3^- + Al(OH)_{3aq} + 3SiO_{2aq} \quad (6b)$$

where $Al(OH)_{3aq}$ + 3 SiO_{2aq} denote the neutral aqueous species of Al and Si in water. Si and Al produced by the albite reaction are removed from the water by precipitation of new Al–silicate minerals including mica and zeolites in fissures (Weisenberger & Bucher, 2010). The dissolution rate of albite increases in carbonate solutions (Chou & Wollast, 1984; Helgeson et al., 1984).

Muscovite (sericite) and other K-fixing sheet silicates (smectite, illite) are typically present in many fractures and fissures of the tunnel. The observed abundant sericite replacing K-feldspar formed from the Al-balanced net-reaction (rxn 7). This combined feldspar alteration process is also balanced with K. Potassium released by Kfs is captured by sericite precipitation. This is consistent with low potassium in the sampled waters (Additional file 1: Table S1).

$$KAlSi_3O_8 + 2NaAlSi_3O_8 + 2H^+ = KAl_3Si_3O_{10}(OH)_2 + 6SiO_{2aq} + 2Na^+ \quad (7)$$

Feldspar hydrolysis producing muscovite / sericite (rxn 7) increases pH and Na in solution. Feldspar dissolution also releases aqueous silica (SiO_{2aq}) to the water. It may accumulate to > 55 mg L^{-1} dissolved SiO_2 in high pH-water (Fig. 9) before quartz-saturation is reached. PHREEQC models for water at 45 °C and TIC (C(4)) = 1 mmol L^{-1} at equilibrium of reaction 7 predict a pH of ~ 10.13, Na = 43 mg L^{-1} and SiO_2 = 55 mg L^{-1}. This is remarkably close to the observed composition of typical water in gneissic and granitic basement. Though, predicted K is ~ 0.1–0.2 mg L^{-1} instead of observed ~ 0.5–1.5 mg L^{-1}. The model correctly predicts that K is much lower than Na in all water from the basement. However, observed K is somewhat higher than predicted equilibrium K. Consequently, computed equilibrium temperature from the Na–K thermometer are near 100 °C instead of 45 °C for most water. Above we concluded that this could indicate that water is not at full equilibrium with the exposed solids at the fracture surfaces. Other contributions to the observed mismatch between observed and modeled K concentration could relate the analytical uncertainty of analyzing K concentrations at the 1 mg L^{-1} level or lower. Furthermore, the elevated K concentration could be a consequence of secondary limited exchange of Na by K at the surfaces of newly formed potassium sheet silicates. The PHREEQC model also suggests undersaturation for the clay minerals kaolinite and beidellite. Including biotite in the PHREEQC model results in similar K concentrations in the solution and as observed very low dissolved Mg.

Calcium: Ca in waters from the crystalline basement originates mainly from the alteration of anorthite component of plagioclase. Ca is removed from the water by precipitation of observed zeolite (laumontite or Ca-rich stilbite). Dissolution of minerals from Ca-silicate lenses or amphiboles from amphibolite occurring in some units of the Gotthard Massif may contribute additional Ca locally (Additional file 1: Table S1). Despite the generally low Ca-concentrations the tunnel-waters are saturated with respect to calcite. Observed calcite on fracture surfaces and in veins and dissolution of secondary calcite coating these fractures are the expected consequences of local dissolution or precipitation of calcite.

Fluoride: Alteration of biotite present in most basement rocks releases Mg, Fe, K and F to the solution. Additional Fe-sources are pyrite and Fe–Mg silicates other than biotite in some rocks. Biotite dissolution is the only significant source of fluorine in the water. Fluoride is a substantial component of the basement waters from the Gotthard Massif. Its presence proves that biotite dissolution progresses along the flow path of the surface water to the sampling fracture in the tunnel. The Bt-dissolution reaction (rxn 8) is essential to the chemical evolution of the water:

$$K(Mg,Fe)_3AlSi_3O_{10}(F)_2 + 5H^+ = K^+ + 3(Mg,Fe)^{2+} + Al(OH)_{3aq} + 3SiO_{2aq} + H_2O + 2F^- \quad (8)$$

Biotite is written here as F-endmember (see below). The basement water contains very little Mg and almost no Fe (Table 1). This means that all Mg and Fe released by

Table 1 Major component characteristics of water in geological units of the Sedrun section (based on % meq L^{-1})

Unit	Prime Cation	Prime Anion	Secondary Cation	Secondary Anion	Major Unit[a]
S-granite-gneiss	Ca	SO_4	Na	F/Cl	Aar Massif
Clavaniev zone	Na	SO_4	Ca	HCO_3/CO_3	cover
TZM north	Na	SO_4	–	HCO_3/CO_3	Tavetsch Massif
TZM south	Na	HCO_3/CO_3	–	Cl/SO_4	Tavetsch Massif
Urseren-Garvera zone	Ca,Mg	HCO_3/CO_3	–	SO_4	cover
Paragneiss	Na	HCO_3/CO_3	–	$F/Cl/SO_4$	Gotthard Massif
Streifen gneiss north	Na	HCO_3/CO_3	Ca	$F/Cl/SO_4$	Gotthard Massif
Paradise gneiss	Na	HCO_3/CO_3	Ca	$F/Cl/SO_4$	Gotthard Massif
Streifen gneiss south	Na	HCO_3/CO_3	Ca	F/SO_4	Gotthard Massif
Piz Fuorcla zone	Na	HCO_3/CO_3	–	F/SO_4	Gotthard Massif
Streifen gneiss s.s	Na	HCO_3/CO_3	Ca	F/SO_4	Gotthard Massif

[a] Major unita: Aar Massif, Gotthard Massif = Variscan or older basement rocks, predominantly gneiss and granite; Cover unit = post-Variscan (Carboniferous-Triassic) meta-sediments

reaction rxn 8 is redistributed into a low-solubility solid. This Mg-Fe sink is predominantly chlorite, which is an abundant product mineral in fissures, fractures and cavities. Released K and excess Mg, Fe are trapped in low-T sheet silicate including various clays (illite, smectite). A generic model for the process is given as reaction 9:

$$2K(Mg,Fe)_3AlSi_3O_{10}(F)_2+4H_2O = (Mg,Fe)_5Al_2Si_3O_{10}(OH)_8+(Mg,Fe)^{2+}+2K^{+}+3SiO_2+4F^{-} \quad (9)$$

Biotite from Streifengneiss s.s. at the south end of the Sedrun section contains up to 0.9 wt% F corresponding to 20 mol.% F-endmember Bt. Since product chlorite does not incorporate F in its structure all F from Bt alteration is released to the water. Streifengneiss biotite also contains a small amount of Cl, typically 0.15 wt% Cl corresponding to ~ 4 mol.% Cl-endmember (analyzed samples from km 27.339). Biotite alteration also contributes a part of the Cl in water. Muscovite present in gneiss contains from 0.2 to 0.4 wt% F and trace amounts of Cl. Ms does not release F to the water because Ms remains in the rock and does not alter to a low-grade product mineral like biotite does. The minor mineral titanite, which is occasionally present, contains 1.7 wt% F and traces of Cl (< 0.01 wt%). Consequently, the F-content of the water directly indicates the extent of Bt-alteration and thus the local brittle deformation, fracturing and faulting. Therefore, Bt-alteration and associated F-release is favored in the same zones that also open primary salty fluid-inclusions in quartz. This explains why fluoride and chloride are correlated (Fig. 8).

The chloride-fluoride signature of water in basement rocks is a sensitive property monitoring the rock unit it is in contact with (Fig. 15). The Cl and F concentrations reflect details of the lithological structure of basement units that are difficult to map in the field or recognize in the opened tunnel. The base of the GM in the north produces very halogen-rich water, probably as a result of massive brittle Alpine deformation. Further south a homogeneous subunit of Paragneiss releases water with markedly lower halogen. The inflows in the following section in Paragneiss and Streifen-Gneiss have similar halogen signatures. It follows a marked zone very low in halogens but has been identified and mapped as Streifen-Gneiss north as well (marked with a darker signature in Fig. 15). The signal could be a result of primary properties of the rock, which might constitute a separate unit. This is our preferred interpretation because TDS and Na do not show a noticeable signal in this zone precluding the possibility that the zone is a low-deformation zone. The inflows distinctly mark the Paradise-Gneiss unit (Fig. 15). Further south all inflows contain more fluoride

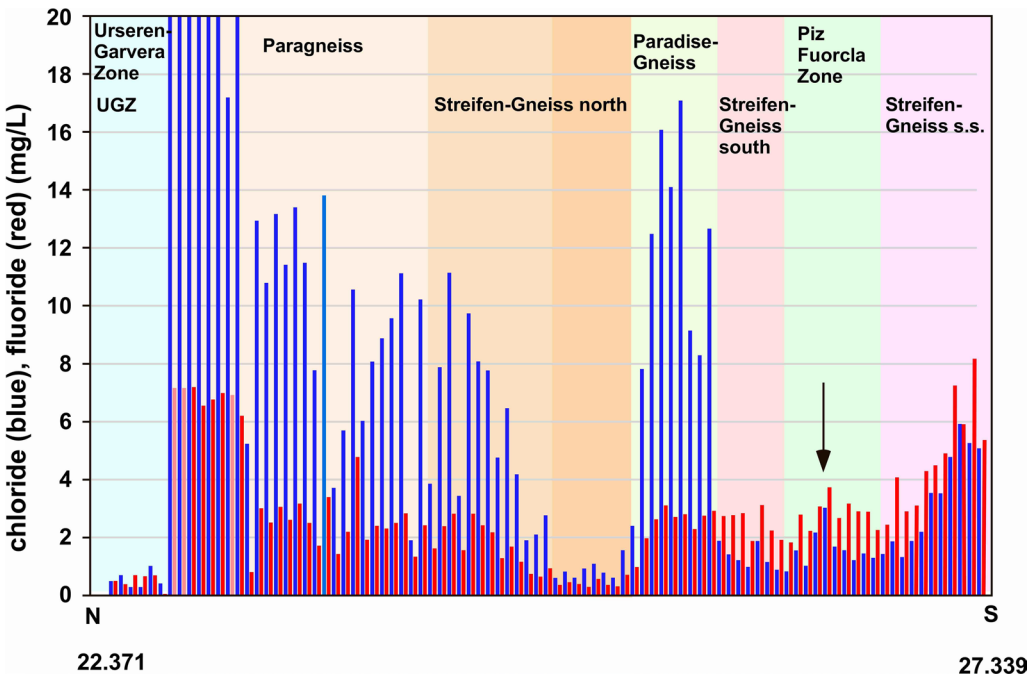

Fig. 15 Chloride and fluoride concentration (mg L^{-1}) measured in Gotthard-Massif inflows in the Gotthard Base Tunnel (Sedrun Section)

than chloride as a result of the high F-content of biotite in these rocks.

The maximum concentration of fluoride is limited by the saturation with fluorite thus by the amount of Ca in the water, which is extremely low in the GM. However, all water-samples from the investigated tunnel section are undersaturated with respect to fluorite (CaF_2) and the occurrence of fluorite is not documented in the GM (in contrast to the Aar-Massif of the Amsteg Section of the tunnel).

Chloride in deep groundwater residing in basement units has potentially 4 sources: It may represent stored fossil seawater, dissolution of evaporitic halite, and alteration of Cl-bearing silicates e.g. biotite or amphibole, but could also be the result of cracked fluid inclusions. The measured range of Cl/Br mass ratios of 20–60 in the northern GM and 40–80 in the southern GM is typical for the salinity in crystalline basement originating from stored brine in original fluid inclusions trapped at high metamorphic temperature mostly in quartz (Stober & Bucher, 1999).

Magnesium: In the southern part of TZM-south relatively high Mg-concentrations were observed (11.7 mg L^{-1}, 21.868 km) where Ca is also elevated (56.8 mg L^{-1}) (Fig. 7). This could be related to the presence of altered ultrabasic lenses in this unit, or more probable to infiltration of dolomite water from the UGZ.

Iron: Measurable Fe concentrations in water from the GM suggest generally reducing conditions consistent with relatively high sulfate from sulfide oxidation (Fe up to 0.7 mg L^{-1}; detection limit 0.02). Fe sources are pyrite, biotite, and amphibole. The tunnel waters are supersaturated with respect to hematite (Fe_2O_3) and goethite. Hematite on fracture surfaces and as fissure deposits is common in the Sedrun region. In the Aar Massif Fe in solution is typically below detection limit of 0.02 mg L^{-1} (Bucher et al., 2012).

Sulfate is an important anion also in waters from the basement rocks (Fig. 6b). Sulfate could be released to the fracture water by dissolution of secondary $CaSO_4$ in fractures of the basement rocks. The second source of sulfate is oxidation of sulfide e.g. pyrite (FeS_2) (rxn 2, 3, 4). The data show that Ca and SO_4 are uncorrelated and Ca/SO_4 is < 1 (mmol L^{-1} ratio) in all samples collected in crystalline basement rocks suggesting that dissolution of gypsum or anhydrite (or gypsum) is not the prime source of sulfate. This conclusion is consistent with the absence of reported gypsum or anhydrite in the Sedrun tunnel (Guntli et al., 2016). Thus sulfate in basement water has the same origin as in the meta-sediments of the UGZ described above, specifically from sulfide dissolution and oxidation. All analyzed rock samples of Streifengneiss and gneiss from the Piz-Fuorcla-Zone contain pyrite. Some also contain secondary calcite and graphite in veinlets and as fracture fillings. Small amounts of methane have been detected in a few selected water samples. H_2S was below detection limit (0.005 mg L^{-1}) and residual O_2 is low. The gas-analysis of one sample from Streifengneiss north revealed CO_2 7943 vol. ppm, O_2 9.0 vol. %, N_2 90.2 vol. %, CH_4 302 vol. ppm (Atmosphere: 380, 20.9, 78.2, 1.5). The reactions that produce sulfate can be written slightly different from for the sulfate produced in the UGZ presented above. Reaction rxn 2 from above dissolves pyrite and the water contains abundant dissolved Fe(II). The iron may subsequently precipitate as siderite (rxn 10):

$$Fe^{2+} + 2HCO_3^- \Rightarrow FeCO_3 + H_2O + CO_2 \quad (10)$$

Siderite occurs on fractures and fissures instead of being oxidized to hematite. The limiting factor keeping Fe in solution is remaining O_2 in water. Alternatively, the ferrous iron may subsequently be oxidized to ferric iron, precipitating as iron oxide, ferric oxyhydroxide, or hydroxide by reactions of the type rxn 11:

$$4FeS_2 + 15HCO_3^- = 2Fe_2O_3 + 8SO_4^{2-} + 7H_2O + 1H^+ + 15C \quad (11a)$$

$$8FeS_2 + 15HCO_3^- + 31H_2O = 4Fe_2O_3 + 16SO_4^{2-} + 17H^+ + 15CH_4 \quad (11b)$$

The significance of both reactions is supported by the abundant occurrence of massif graphite coatings on many fracture surfaces and by the presence of methane in the water. The acidity produced bey the process (rxn 11) can be buffered by dissolving vein calcite or by silicate hydrolysis reactions. As a consequence pH and sulfate data (Table 1) do not correlate.

In addition to the dissolved CO_2 in meteoric water (rxn 11) the limiting factor for sulfate production from sulfide minerals is the initial amount of dissolved oxygen in the meteoric recharge (rxn 4). Meteoric water contains 354 mmol L^{-1} O_2 in equilibrium with the atmosphere. Thus it can produce water with a maximum of 58 mg L^{-1} sulfate. The waters are generally below this limit. All water south of the major fault at km 22.77 marking the northern contact of the Gotthard Massif have sulfate exclusively derived from dissolution and oxidation of sulfide minerals. The boundary fault itself conducts water with the record amount of ~ 2500 mg L^{-1} sulfate. In the UGZ SO_4 is below 57 mg L^{-1}. The TZM south is very low in sulfate. At km 20.285 within TZM south there is a sharp increase in sulfate towards north with a marked peak at km 19.650 in TZM north with 1330 mg L^{-1} SO_4.

Within the CZ and the Aar Massif SO_4 is far above 57 mg L^{-1}. At the high sulfate inflows SO_4 has an additional source other than sulfide dissolution and oxidation. Since the high-sulfate inflows are not restricted to the meta-sediments of the Clavaniev Zone but are typical also of the Aar Massif basement the origin is not simply dissolution of evaporitic anhydrite. Furthermore in the Urseren-Garvera-Zone with its dolomitic marbles SO_4 is very low and anhydrite is not a source of sulfate. However, anhydrite occurring on fissures and fractures in basement rocks of the Aar Massif is a proven source of SO_4 in the Amsteg section of the tunnel (Bucher et al., 2012).

Potassium concentrations are generally very low in all tunnel waters. The prime source of K in solution is dissolution of K-feldspar and alteration of biotite. Biotite dissolution releases more K than F to the water and the two solutes correlate according to the mean Bt composition in a rock unit. However, no K–F correlation was found, molar F is always much higher than K. This finding suggests that K is removed from the water by precipitating new minerals such as illite and trapped in zeolites, stilbite for example (Bucher & Weisenberger, 2013). Additionally by adsorptive fixation to clay mineral surfaces may decrease K relative to F.

Inorganic carbon: The source of TIC is atmospheric CO_2 dissolved in infiltrating recharge. CO_2 decreases along the fracture flow path accompanied by increasing pH. In some rocks dissolution of secondary calcite on fractures and in veins contributes to TIC.

7.2.2 Permeability variation and its consequences for the composition of deep water

The natural permeability differs significantly between the basement massifs and between different units within the basement. This relates to a considerably higher frequency of water inflow zones (fractures, fissures, faults, etc.) with generally higher flow rates in the investigated tunnel section of the Aar Massif compared to the Gotthard-Massif (Guntli et al., 2016; Masset & Loew, 2013). Local fault zones with massively enhanced permeability occur also in the GM. The most prominent of these zones forms the northern terminus of the Gotthard Massif at km 22.659 (Figs. 2, 5, 7). Yet, the amount of infiltrating meteoric water (containing CO_2) in the Aar Massif is generally higher, leading to higher fluid-rock alteration, water with significantly higher TDS and distinctly different composition compared to the Gotthard Massif. The higher CO_2 supply in the Aar Massif waters at tunnel level leads to generally higher Ca- and TIC-contents. The findings are in agreement with laboratory alteration experiments on granitic material in CO_2-free and CO_2-rich fluids (Bucher & Stober, 2002) and with observations in natural settings with ascending CO_2–rich springs (Bucher & Stober, 2000).

Prominent zones of increased permeability correlate with pronounced signals in water composition (Figs. 5, 7). The strongly deformed meta-sediments of the Clavaniev-zone release water with a moderately increased TDS associated with a Ca-buildup (#1 on Figs. 5, 7). A very marked TDS, Na and Cl upsurge occurs at ~ km 19.8 (#2 on Figs. 5, 6). It is located below the deepest point of the Rhine river valley. The concentration peaks are probably not related to the properties of the rocks of the TZM north unit but reflect the highly permeable north rim of the TZM and a flow of deep groundwater under the Rhine River. The direction of the valley and groundwater flow is from W to E normal to the tunnel and the sections shown on the figures. The minor concentration peak (#3 on Figs. 5, 6) at ~ km 21.9 is related to a zone of deformed granitoid dykes and amphibolites in the TZM basement that also marks a fracture zone with enhanced permeability. The contact between the UGZ (cover of TZM) and the base of the Gotthard Massif at ~ km 22.659 is the most prominent fault and fracture zone along the Sedrun section (#4 on Figs. 5, 6). In this fault zone water with the most extreme composition have been collected from the massive inflow. TDS exceeds 3.6 g L^{-1}. The composition in mg L^{-1}: Ca 426, Na 638, SO_4 2440. It is 10—20 times higher than at the neighboring inflows in the UGZ and GM respectively. pH and TIC are relatively low. The water has characteristics of both, the marbles and sulfide-rich schists of the UGZ and the Paragneiss of the GM. The massive composition anomaly is related to the drastically enhanced permeability along the fault (see above Sect. 6.1; Fig. 12). With the basement gneiss units of the Gotthard Massif two further zones with enhanced permeability occur (#5 on Figs. 5, 6; #6 on Fig. 5). In the Paradise-gneiss unit a prominent Cl associated with a distinct Na peak occurs (~ km 26). Since Cl mainly originates from cracked and opened primary salty fluid-inclusions the observed NaCl peak is probably related to enhanced fracture deformation within this zone. A similar yet less prominent Cl-peak occurs at ~ km 24.7 at the boundary between Paragneiss and Streifen-gneiss. Increased Cl reflects the increased permeability; the Na signal is lost in the background Na content of the water, which is related to the hydrolysis of albite.

7.2.3 The role of zeolites

Zeolites are abundant in fissures of the basement massifs (Amacher & Schüpbach, 2011; Bucher & Weisenberger, 2013; Stalder et al., 1980; Weisenberger & Bucher, 2010). The prime zeolites are laumontite and stilbite, but also heulandite, scolecite, chabazite occur in fissures of the basement rocks. Zeolites form by the Al-Si transfer

reaction plagioclase = Ca–zeolite + albite or in a more general process formulation granite + water 1 = zeolite + chlorite + water 2 (Weisenberger & Bucher, 2010). The zeolite forming reactions do not change pH of the reacting water. All zeolite analyzed from the basement massifs are Ca–zeolites containing very little Na except for late stilbite. However, chabazite and heulandite contain a considerable amount of potassium (up to 1.5 wt% K; Weisenberger & Bucher, 2010). Newly formed Ca–zeolites capture some of the K released by the biotite alteration.

All tunnel-waters are strongly supersaturated with respect to Ca–zeolite minerals. The highest saturation indexes (SI values) have been computed for stilbite, implying that stilbite is the stable zeolite phase under the present day conditions (T up to 50 °C). Stilbite from the road tunnel through the Gotthard Massif to the west of the Sedrun section of the base-tunnel and from the Aar Massif of the Amsteg section of the base-tunnel vary in composition between pure Ca-stilbite (stellerite) and stilbite s.s. with close to 20 mol % Na-Stb (Bucher & Weisenberger, 2013).

7.3 Interpretation of data from time series.

7.3.1 Röti formation site (UGZ)

Water from the inflow in the Röti formation is simply controlled by the dolomite dissolution reaction (rxn 1) (Additional file 1: Table S1). The secondary anion sulfate is produced from the sulfide oxidation reactions (rxn 2–5) formulated and discussed above. The first sample from the Röti inflow point (UGZ) was taken in 2006 right after excavation of the tunnel. The composition of this water is closest to the original water residing in the undisturbed fractured marble. The pre-tunnel conditions were characterized by a near equilibrium pressure distribution and by extremely slow fluid flow. Numerical models of the pre-tunnel flow systems for the situation of the Amsteg section suggested that the flow velocity of the fluid was on the order of 2 m $year^{-1}$ (Wanner et al., 2018). The Sedrun section has similar overburden but significantly smaller elevation gradients. The expected flow rates are thus smaller, probably much smaller, than in the Amsteg section. The hydraulic gradients increased dramatically after drilling the tunnel resulting in 0.10 L s^{-1} produced water initially. The discharge tripled over time to 0.32 L s^{-1} until the last sample was taken in 2010. This suggests that the fracture apertures increased as result of dissolution of dolomite and calcite on the fractures surfaces enlarging the hydraulic conductivity of the system. The excavation of the tunnel changes the hydraulic potential of the mountain and the tunnel acts hydraulically as a sink.

During recharge meteoric water infiltrates the ground at the surface and migrates along the very steeply dipping UGZ meta-sediments and reaches the UGZ at tunnel level (Fig. 2). Along its steep flow path, the water is in contact mainly with dolomite of the relatively permeable Röti formation and pyrite in the Liassic shales. CO_2 and O_2 are transported from the surface with the infiltrating water. With increasing depth CO_2 and O_2 is consumed successively due to interaction with the surrounding rock in the UGZ.

The chemical composition of the water at the Röti inflow changes progressively towards compositions typical of water from closer to the surface. Ca, Mg, and SO_4 increase because the water is increasingly loaded with unreacted CO_2 and O_2 from the atmosphere. Consequently with increasing time TDS of the inflow increases.

7.3.2 Paragneiss site of Gotthard-Massif (km 23.676)

Water from a fault at km 23.676 collected during 935 days (fall 2006–spring 2009) show increasing concentrations for Na, TIC, H, and TDS. After 153 days the inflow drastically decreased from 5 L s^{-1} and nearly stopped after 237 days (0.1 L s^{-1}). The reduction in flow rate was not accompanied with drastic changes in water composition. Later the inflow increased to about 2–3 L s^{-1}. The incident that caused the changes in the flow rate is unknown. The event is clearly visible, however, in the concentration of the minor components chloride (Fig. 13) and fluoride. Both Cl and F dropped drastically at the time of the flowrate drop (Cl from 16 to 8 mg L^{-1}; F from 3.2 to 2 mg L^{-1}). After inflow picked up again at a lower temperature the water was increasingly loaded with unreacted CO_2 and O_2 from the surface.

8 Summary and conclusions

211 water samples collected from water inflow points in the central section of the Gotthard Base Tunnel up to 2350 m below surface are all of meteoric origin and evolved solely due to chemical interaction with granite and gneiss of prealpine basement and a few zones of steeply dipping metasediments along their infiltrating flow path.

The deep water in the crystalline basement of the continental upper crust representatively exposed in the Gotthard tunnel acquire their dissolved solids by dissolving of albite-rich plagioclase, K-feldspar, Fe–sulfide oxidation, alteration of biotite, and from leaching of soluble inclusions in pores and in minerals. The reactions dissolve minerals of the granitoid rocks exposed on the fracture surfaces of fissures and faults. The solid products of the solute producing reactions include zeolite, chlorite and other clay minerals and carbon

(graphite and/or amorphous carbon). The remarkably wide variation of water composition (Table 1, Additional file 1: Table S1) has been generated by the interaction of meteoric water with rather uniform rock types in the crystalline basement (gneisses, schists) consisting predominantly of K-feldspar, plagioclase, quartz and biotite.

Water in the meta-sediments of the Urseren-Garvera-Zone differs considerably from those in the crystalline basement. The Ca-Mg-carbonate water results from interaction with calcite-dolomite marbles and pyrite-graphite schists.

Basement units (Aar and Gotthard Massif) differ significantly. Due to the higher fracture permeability of the Aar Massif, more meteoric water (containing O_2 and CO_2) infiltrates even deeper parts of the crystalline basement. Thus in the Gotthard Massif CO_2 is a limiting factor for alteration processes and tunnel waters have lower TDS and significant compositional differences.

Other causes of the compositional variation are modal variations in mica (biotite, muscovite) and pyrrhotite / pyrite content. The latter limits the total amount of sulfate that can be released to the water and also controls the consumption of TIC as oxidizing substances for sulfate generation. Despite the slow reaction kinetics in low T-environments, silicate dissolution provides most of the sodium (Na) and all dissolved silica and fluorine of the basement waters in the tunnel.

With increasing time, inflow of water into the tunnel will progressively reflect the composition of water typical of the shallower parts of the overburden with lower temperature and a smaller amount of dissolved SiO_2. The portion of shallow water from higher up in the overburden increases with time. The colder near-surface water is 'younger' and contains atmospheric CO_2, which converts to dissolved carbonate (HCO_3 and CO_3) along its flow path to tunnel level. Water from the upper part of the overburden has a lower pH. With increasing depth CO_2 is consumed successively by hydrolysis reactions with silicates of the fractured rock thereby increasing pH.

The data clearly show that in the depth interval of 1.0–2.5 km below surface deep water in continental basement evolves to a low TDS, high pH, sodium carbonate and silica solution by interaction of gneiss and granite with infiltrating pristine meteoric water, snowmelt and rain.

Supplementary Information

The online version contains supplementary material available at https://doi.org/10.1186/s00015-022-00413-0.

Additional file 1: Table S1. Hydrochemical analyses of tunnel waters in the investigated section of the Gotthard-Base-Tunnel, analyzed by IMPG, University of Freiburg.

Acknowledgements
AlpTransit Gotthard AG is thanked for providing access to the tunnel and supplying water samples. The help and support by the tunnel geologists is gratefully acknowledged. We thank Helmer Schack-Kirchner from Soil-Science Freiburg for gas analyses. The constructive and helpful comments and suggestions by two anonymous reviewers are acknowledged with gratitude.

Authors contributions
IS carried out fieldwork, analyzed and interpreted the hydraulic test and hydrochemical data, drafted the figures, tables, and the manuscript. FG carried out fieldwork, assembled chemical data, and supported the investigation in the tunnel. VW carried out fieldwork, analyzed and assembled chemical data. KB analyzed and interpreted geochemical data and prepared the revised version of the manuscript. IS and KB approved the final submission. All authors read and approved the final manuscript.

Funding
Open Access funding enabled and organized by Projekt DEAL.

Availability of data and materials
All relevant data generated or analyzed during this study are included in this published article. Additional data are available from the corresponding author on reasonable request.

Declarations

Ethics approval and consent to participate
Not applicable.

Consent for publication
All authors have given their consent for publication.

Competing interests
The authors declare that they have no competing interests.

Author details
[1]Institut für Geo- und Umweltnaturwissenschaften, Albert-Ludwigs-Universität Freiburg, Albertstr. 23B, 79104 Freiburg, Germany. [2]CSD Ingenieure AG, Compognastrasse 30, 7430 Thusis, Switzerland.

Received: 21 October 2021 Accepted: 14 February 2022
Published online: 24 March 2022

References

Akcil, A., & Koldas, S. (2006). Acid Mine Drainage (AMD): Causes, treatment and case studies. *Journal of Cleaner Production, 14*, 1139–1145.
Amacher, P. & Schüpbach, T. (2011). NEAT-Mineralien, Kristallschätze tief im Berg. *GEO-Uri GmbH Verlag*, 233 p., Amsteg. ISBN: 978-3-033-03111–1
Aquilina, L., Pauwels, H., Center, A., & Fouillac, C. (1997). Water-rock interaction processes in the Triassic sandstone and the granitic basement of the Rhine Graben: Geochemical investigation of a geothermal reservoir. *Geochimica Et Cosmochimica Acta, 61*, 4281–4295.
Aquilina, L., Sureau, J. F., & Steinberg, M. (1997). Comparison of surface-, aquifer- and pore-waters from a Mesozoic basin and its underlying Palaeozoic basement, southeast France: Chemical evolution of waters and relationships between aquifers. *Chemical Geology, 138*, 185–209.
Belgrano, T. M., Herwegh, M., & Berger, A. (2016). Inherited structural controls on fault geometry, architecture and hydrothermal activity: An example from Grimsel Pass, Switzerland. *Swiss Journal of Geosciences, 109*, 345–364.
Bucher, K., & Stober, I. (2000). The composition of groundwater in the continental crystalline crust. In I. Stober & K. Bucher (Eds.), *Hydrogeology in crystalline rocks* (pp. 141–176). KLUWER Academic Publishers.

Bucher, K., & Stober, I. (2002). Water–rock reaction experiments with Black Forest gneiss and granite. In I. Stober & K. Bucher (Eds.), *Water–rock interaction* (pp. 61–96). KLUWER Academic Publishers.
Bucher, K., & Stober, I. (2010). Fluids in the upper continental crust. *Geofluids, 10*, 241–253.
Bucher, K., Stober, I., & Seelig, U. (2012). Water deep inside the mountains: Unique water samples from Gotthard rail base tunnel, Switzerland. *Chemical Geology, 334*, 240–253.
Bucher, K., & Weisenberger, T. B. (2013). Fluid-induced mineral composition adjustments during exhumation: The case of Alpine stilbite. *Contributions to Mineralogy and Petrology, 166*, 1489–1503.
Bucher, K., Zhang, L., & Stober, I. (2009). A hot spring in granite of the Western Tianshan, China. *Applied Geochemistry, 24*, 402–410.
Bucher, K., Zhou, W., & Stober, I. (2017). Rocks control the chemical composition of surface water from the high Alpine Zermatt area (Swiss Alps). *Swiss Journal of Geosciences, 110*, 811–831.
Chou, I., & Wollast, R. (1984). Study of the weathering of albite at room temperature and pressure with a fluidized reactor. *Geochimica Et Cosmochimica Acta, 48*, 2205–2217.
Cooper, H. H., & Jacob, C. E. (1946). A generalized graphical method for evaluating formation constants and summarizing well-field history. *Transactions of the American Geophysical Union, 24*(4), 526–534.
Craig, H. (1961). Isotopic variations in meteoric waters. *Science, 133*(3465), 1702–1703.
Craw, D., Koons, P. O., Zeitler, P. K., & Kidd, W. S. F. (2005). Fluid evolution and thermal structure in the rapidly exhuming gneiss complex of Namche Barwa-Gyala Peri, eastern Himalayan syntaxis. *Journal of Metamorphic Geology, 23*, 829–845.
Diamond, L. W., Wanner, C., & Waber, H. N. (2018). Penetration depth of meteoric water in orogenic geothermal systems. *Geology, 46*, 1063–1066.
Dietermann, N. (2010). Stabile Isotope im Schnee: Räumliche und zeitliche Variabilität. Unpublished Master thesis, University of Freiburg, 158 S. Freiburg.
Edmunds, W. M., Kay, R. L., & McCartney, R. A. (1985). Origin of saline groundwaters in the Carnmenellis granite (Cornwall, England): Natural processes and reaction during hot dry rock reservoir circulation. *Chemical Geology, 49*, 287–301.
Forster, C., & Smith, L. (1988). Groundwater flow systems in mountainous terrain: 2 Controlling Factors. *Water Resources Research, 24*, 1011–1023.
Frape, S. K., Blyth, A., Blomqvist, R., McNutt, R. H., & Gascoyne, M. (2004). Deep fluids in the continents: II. Crystalline rocks. In J. I. Drever, H. D. Holland, & K. K. Turekian (Eds.), *Surface and ground water, weathering, and soils: Treatise on geochemistry* (pp. 541–580). Elsevier.
Frey, M., Bucher, K., & Mullis, J. (1980). Alpine metamorphism along the Geotraverse Basel-Chiasso—A review. *Eclogae Geologicae Helvetiae, 73*, 527–546.
Gascoyne, M. (2004). Hydrogeochemistry, groundwater ages and sources of salts in a granitic batholith on the Canadian Shield, southeastern Manitoba. *Applied Geochemistry, 19*, 519–560.
Ge, S., Wu, Q. B., Lu, N., Jiang, G. L., & Ball, L. (2008). Groundwater in the Tibet Plateau, western China. *Geophysical Research Letters, 35*, L18403.
Goderniaux, P., Davy, P., Bresciani, E., de Dreuzy, J.-R., & Le Borgne, T. (2013). Partitioning a regional groundwater flow system into shallow local and deep regional flow compartments. *Water Resources Research, 49*, 2274–2286.
Grasby, S. E., Ferguson, G., Brady, A., Sharp, C., Dunfield, P., & McMechan, M. (2016). Deep groundwater circulation and associated methane leakage in the northern Canadian Rocky Mountains. *Applied Geochemistry, 68*, 10–18.
Grimaud, D., Beaucaire, C., & Michard, G. (1990). Modelling of the evolution of ground waters in a granite system at low temperature: The Stripaground waters, Sweden. *Applied Geochemistry, 5*, 515–525.
Gruber, L. R., & Holstein, U. (2016). Konventionelle Vortriebe Sedrun (conventional tunnel drives at Sedrun). *Geomechanics and Tunnelling, 9*(2), 111–128.
Guntli, P. (2005). Vortrieb Gotthard-Basistunnel, Teilabschnitt Sedrun: geologisch-geotechnisch-hydrogeologische Verhältnisse im Tavetscher Zwischenmassiv und in der Urseren-Garvera-Zone. In: Löw, S. et al. (eds.), Geologie und Geotechnik der Basistunnel am Gotthard und am Lötschberg, *Proc. intern. symp. Geologie* AlpTransit 2005, Zürich. Zürich/Singen: vdf Hochschulverlag AG.
Guntli, P., Keller, F., Lucchini, R. & Rust, S. (2016). Gotthard-Basistunnel: Geologie, geotechnik, hydrogeologie—zusammenfassender Schlussbericht. *Berichte der Landesgeologie*, **7**, 180, Wabern/Schweiz.
Helgeson, H. C. (1979). Mass transfer among minerals and hydrothermal solutions. In H. L. Barnes (Ed.), *Geochemistry of hydrothermal ore deposits* (pp. 568–610). John Wiley.
Helgeson, H. C., Garrels, R. M., & Mackenzie, F. T. (1969). Evaluation of irreversible reactions in geochemical processes involving minerals and aqueous solutions—II. Applications. *Geochimica Et Cosmochimica Acta, 33*, 455–481.
Helgeson, H. C., Murphy, W. M., & Aagaard, P. (1984). Thermodynamic and kinetic constraints on reaction rates among minerals and aqueous solutions. *Geochimica Et Cosmochimica Acta, 48*, 2405–2432.
Hubbert, M. K. (1940). The theory of groundwater motion. *The Journal of Geology, 48*, 785–944.
Ingebritsen, S. E., & Manning, C. E. (1999). Geological implications of a permeability-depth curve for the continental crust. *Geology, 27*, 1107–1110.
Leu, W., & Wyss, R. (1992). Geologische Aufnahme und Prognoseprofil im Gebiet von Sedrun Vorderrheintal. *Vereinigung Schweizerischer Petroleum Geologen Und Ingenieure Bulletin, 59*(135), 81–92.
Loew, S., Barla, G. & Diederichs, M. (2010). Engineering geology of Alpine tunnels: Past, present and future. 11th IAEG Congress, 35 p., Auckland, New Zealand.
Manning, C. E., & Ingebritsen, S. E. (1999). Permeability of the continental crust: Implications of geothermal data and metamorphic systems. *Reviews of Geophysics, 37*, 127–150.
Masset, O., & Loew, S. (2013). Quantitative hydraulic analysis of pre-drillings and inflows to the Gotthard Base Tunnel (Sedrun Lot, Switzerland). *Engineering Geology, 164*, 50–66.
Mezger, F., Anagnostou, G., & Ziegler, H.-J. (2013). The excavation-induced convergences in the Sedrun section of the Gotthard Base Tunnel. *Tunnelling and Underground Space Technology, 38*, 447–463.
O'Neil, J. R. (1968). Hydrogen and oxygen isotope fractionation between ice and water. *Journal of Physical Chemistry, 72*, 3683–3684.
Parkhurst, D.L., & Appelo, C.A.J. (1999). User's guide to PHREEQC (Version 2)—A computer program for speciation, batch-reaction, one-dimensional transport and inverse geochemical calculations. Water-Resources Investigations Report 99–4259, U.S. Geological Survey, Denver, Colorado, p. 312.
Pastorelli, S., Marini, L., & Hunziker, J. C. (2001). Chemistry, isotope values (dD, $\partial^{18}O$, $\partial^{34}S_{SO4}$) and temperatures of the water inflows in two Gotthard tunnels, Swiss Alps. *Applied Geochemistry, 16*, 633–649.
Pauwels, H., Fouillac, C., & Fouillac, A. M. (1993). Chemistry and isotopes of deep geothermal saline fluids in the Upper Rhine Graben: Origin of compounds and water-rock interactions. *Geochimica Et Cosmochimica Acta, 57*, 2737–2749.
Pearson, F.J., Balderer, W., Loosli, H.H., Lehmann, B.E., Matter, A., Peters, T.J., Schmassmann, H., & Gautschi, A. (1991). Applied isotope hydrogeology—A case study in Northern Switzerland. Nagra tech. Rep. NTB 88–01 Nagra, Wettingen/Switzerland.
Pfeifer, H.R., Sanchez, A., & Degueldre, C. (1992). Thermal springs in granitic rocks from the Grimsel Pass (Swiss Alps): The late stage of a hydrothermal system related to Alpine Orogeny. In: Kharaka, Y.K., Maest, A.S. (eds.), Proceedings of water–rock interaction. A. A. Balkema, pp. 1327–1330.
Reyes, A. G., Christenson, B. W., & Faure, K. (2010). Sources of solutes and heat in low-enthalpy mineral waters and their relation to tectonic setting, New Zealand. *Journal of Volcanology and Geothermal Research, 192*, 117–141.
Seelig, U., & Bucher, K. (2010). Halogens in water from the crystalline basement of the Gotthard rail base tunnel (Central Alps). *Geochimica Cosmochimica Acta, 74*, 2581–2595. https://doi.org/10.1016/j.gca.2010.01.030
Sonney, R., & Vuataz, F.-D. (2009). Numerical modelling of Alpine deep flow systems: a management and prediction tool for an exploited geothermal reservoir (Lavey-les-Bains, Switzerland). *Hydrogeology Journal, 17*, 601–616.
Stalder, H. A., Sicher, V., & Lussmann, L. (1980). *Die Mineralien des Gotthardbahntunnels und des Gotthardstarssentunnels N2* (p. 161). Repof Verlag.
Steck, A., & Hunziker, J. C. (1994). The Tertiary structural and thermal evolution of the Central Alps – compressional and extensional structures in an orogenic belt. *Tectonophysics, 238*, 229–254.
Stichler, W., Schotterer, U., Fröhlich, K., Ginot, P., Kull, C., Gäggelerer, H., & Pouyaud, B. (2001). Influence of sublimation on stable isotope records

recovered from high altitude glaciers in the tropical Andes. *Journal of Geophysical Research, 19*(106), 22613–22620.
Stober, I. (1995). Die Wasserführung des kristallinen Grundgebirges. *Ferdinand Enke Verlag*, 191 p., Stuttgart.
Stober, I. (1996). Researchers study conductivity of crystalline rock in proposed radioactive waste site. *EOS American Geophysical Union*, **77/10**, 93–94, Washington DC.
Stober, I., & Bucher, K. (2021). Geothermal energy, from theoretical models to exploration and development. 2nd edition. Springer-Verlag Berlin Heidelberg, pp. 390. ISBN 978–3–030–71684–4. https://doi.org/10.1007/978-3-030-71685-1_1
Stober, I., & Bucher, K. (1999). Origin of salinity of deep groundwater in crystalline rocks. *Terra Nova, 11*, 181–185.
Stober, I., & Bucher, K. (2005). The upper continental crust, an aquifer and its fluid: Hydraulic and chemical data from 4 km depth in fractured crystalline basement rocks at the KTB test site. *Geofluids, 5*, 8–19.
Stober, I., & Bucher, K. (2007). Hydraulic properties of the crystalline basement. *Hydrogeology Journal, 15*, 213–224.
Stober, I., & Bucher, K. (2015). Hydraulic conductivity of fractured upper crust: Insights from hydraulic tests in boreholes and fluid-rock interaction in crystalline basement rocks. *Geofluids, 15*, 161–178.
Stober, I., Richter, A., Brost, E., & Bucher, K. (1999). The Ohlsbach Plume: Natural release of deep saline water from the crystalline basement of the Black Forest. *Hydrogeology Journal, 7*, 273–283.
Stober, I., Zhong, J., Zhang, L., & Bucher, K. (2016). Deep hydrothermal fluid–rock interaction: The thermal springs of Da Qaidam, China. *Geofluids, 16*, 711–728.
Stotler, R. L., Frape, S. K., Ruskeeniemi, T., Pitkänen, P., & Blowes, D. (2012). Periglacial–glacial cycling and the geochemical evolution of Canadian Shield groundwaters. *Geochimica Et Cosmochimica Acta, 76*, 45–67.
Taillefer, A., Guillou-Frottier, L., Soliva, R., Magri, F., Lopez, S., Courrioux, G., Millot, R., Ladouche, B., & Le Goff, E. (2018). Topographic and faults control of hydrothermal circulation along dormant faults in an Orogen. *Geochemistry, Geophysics, Geosystems, 19*, 4972–4995.
Toth, J. (1963). A theoretical analysis of groundwater flow in small drainage basins. *Journal of Geophysical Research, 68*(16), 4795–4812.
Wanner, C., Waber, H.N., & Bucher, K. (2018). Including stable water isotopologues in large-scale reactive transport simulations of topography-driven flow in fractured crystalline rocks. Proceedings TOUGH Symposium 2018, Lawrence Berkeley National Laboratory, Berkeley, California, October 8–10, 2018, p. 45–49.
Wanner, C., Waber, H. N., & Bucher, K. (2020). Geochemical evidence for regional and long-term topography-driven groundwater flow in an orogenic crystalline basement (Aar Massif, Switzerland). *Journal of Hydrology, 581*, 124374.
Weisenberger, T., & Bucher, K. (2010). Zeolites in fissures of granites and gneisses of the Central Alps. *Journal of Metamorphic Geology, 28*, 825–847.
Weisenberger, T., & Bucher, K. (2011). Mass transfer and porosity evolution during low temperature water–rock interaction in gneisses of the Simano nappe—Arvigo, Val Calanca, Swiss Alps. *Contributions to Mineralogy and Petrology, 162*, 61–81.
Weisenberger, T., Rahn, M., van der Lelij, R., Spikings, R., & Bucher, K. (2012). Timing of low-temperature mineral formation during exhumation and cooling in the Central Alps, Switzerland. *Earth and Planetary Science Letters, 327–328*, 1–8.
Whitney, D. L., & Evans, B. W. (2010). Abbreviations for names of rock-forming minerals. *American Mineralogist, 95*, 185–187.
Wolery, T.J. (1992). EQ3/6, a software package for geochemical modelling of aqueous systems: Package overview and installation guide. *Lawrence Livermore National Laboratory*, Livermore, California.
Zhu, C. (2009). Geochemical modeling of reaction path and geochemical reaction networks. *Reviews in Mineralogy and Geochemistry, 70*, 533–569.

Publisher's Note